Article

Developmental Cell

Two sensory neurons coordinate the systemic mitochondrial stress response via GPCR signaling in *C. elegans*

Graphical abstract

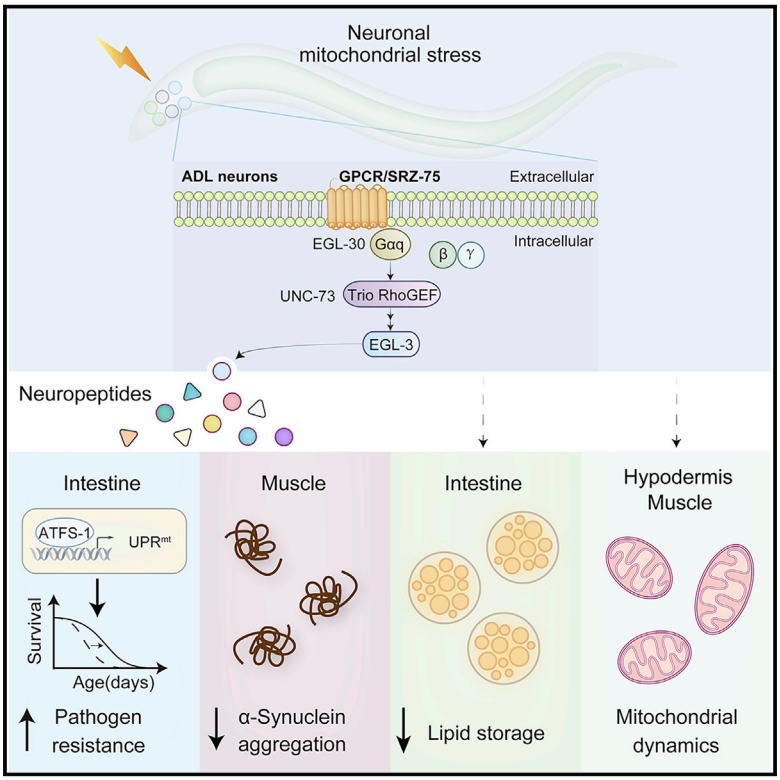

Highlights

- The GPCR SRZ-75 in ADL neurons mediates the systemic UPR^{mt} activation in *C. elegans*
- SRZ-75 couples with Gαq to drive the systemic UPR^{mt} via releasing neuropeptides
- Ablation of ADL neurons attenuates the systemic UPR^{mt} activation
- Enhanced GPCR signaling induces stress resistance and metabolic adaptations

Authors

Yangli Liu, Jun Zhou, Ning Zhang, ..., Wenfeng Zhang, Xinyu Li, Ye Tian

Correspondence

ytian@genetics.ac.cn

In brief

Liu and Zhou et al. find that GPCR SRZ-75 couples Gαq in a pair of ADL chemosensory neurons to coordinate the systemic activation of the mitochondrial unfolded protein response in *C. elegans*. Constitutive activation of Gαq in two ADL neurons alters the physiology of peripheral tissues that improves whole-organismal fitness.

Liu et al., 2022, Developmental Cell *57*, 2469–2482
November 7, 2022
https://doi.org/10.1016/j.devcel.2022.10.001

CellPress

Developmental Cell

CellPress

Article

Two sensory neurons coordinate the systemic mitochondrial stress response via GPCR signaling in *C. elegans*

Yangli Liu,[1,4] Jun Zhou,[1,2,4] Ning Zhang,[1,2] Xueying Wu,[1] Qian Zhang,[1] Wenfeng Zhang,[1,2] Xinyu Li,[1,2] and Ye Tian[1,2,3,5,*]

[1]State Key Laboratory of Molecular Developmental Biology, Institute of Genetics and Developmental Biology, Chinese Academy of Sciences, Beijing 100101, China

[2]University of Chinese Academy of Sciences, Beijing 100093, China

[3]Center for Excellence in Animal Evolution and Genetics, Chinese Academy of Sciences, Kunming 650223, China

[4]These authors contributed equally

[5]Lead contact

*Correspondence: ytian@genetics.ac.cn

https://doi.org/10.1016/j.devcel.2022.10.001

SUMMARY

Mitochondrial perturbations within neurons communicate stress signals to peripheral tissues, coordinating organismal-wide mitochondrial homeostasis for optimal fitness. However, the neuronal control of the systemic stress regulation remains poorly understood. Here, we identified a G-protein-coupled receptor (GPCR), SRZ-75, that couples with Gαq signaling in a pair of chemosensory ADL neurons to drive the mitochondrial unfolded protein response (UPR^{mt}) activation in the intestine via the release of neuropeptides in *Caenorhabditis elegans*. Constitutive activation of Gαq signaling in the ADL neurons is sufficient to induce the intestinal UPR^{mt}, leading to increased stress resistance and metabolic adaptations. Ablation of ADL neurons attenuates the intestinal UPR^{mt} activation in response to various forms of neuronal mitochondrial dysfunction. Thus, GPCR and its Gαq downstream signaling in two sensory neurons coordinate the systemic UPR^{mt} activation, representing a previously uncharacterized, but potentially conserved, neuronal signaling for organismal-wide mitochondrial stress regulation.

INTRODUCTION

The systemic coordination of the metabolic states between different tissues is essential for an organism's overall fitness under stress conditions (Bar-Ziv et al., 2020; Frakes and Dillin, 2017). Mitochondria are the metabolic center and serve as signaling hubs to maintain cellular homeostasis (Andréasson et al., 2019; Pfanner et al., 2019; Spinelli and Haigis, 2018). The mitochondrial unfolded protein response (UPR^{mt}) is activated when mitochondrial proteostasis is disrupted under stress conditions, leading to increased expression of mitochondrial chaperones and proteases, xenobiotic and reactive oxygen species (ROS)-detoxifying genes, and metabolic enzymes to promote the recovery of mitochondrial protein homeostasis and defense against infection (Bar-Ziv et al., 2020; Naresh and Haynes, 2019; Nargund et al., 2012, 2015; Tian et al., 2016b).

The UPR^{mt} is mediated by the transcription factor ATFS-1 (activating transcription factor associated with stress-1), which harbors a mitochondrial localization sequence (MTS) and a nuclear localization sequence (NLS) (Nargund et al., 2012). In the absence of mitochondrial stress, ATFS-1 is imported into the mitochondria where it is degraded by the mitochondrial Lon protease. However, mitochondrial import efficiency is reduced during stress, allowing ATFS-1 to localize to the nucleus where it activates the UPR^{mt} (Nargund et al., 2012, 2015). In addition to ATFS-1, other proteins are also critical for the activity of the UPR^{mt}, including the transcription factor DVE-1 (homolog to the human SATB2), and the epigenetic factors such as histone methyltransferase MET-2/LIN-65, and the nucleosome remodeling and deacetylase (NuRD) complex (Haynes et al., 2007; Li et al., 2021; Shao et al., 2020; Tian et al., 2016a; Zhu et al., 2020, 2022).

For metazoans, mitochondrial stress from one tissue can induce a UPR^{mt} in distal tissues via cell-non-autonomous signaling, allowing organisms to better cope with local mitochondrial perturbations (Bar-Ziv et al., 2020; Morimoto, 2020). For example, neuronal knockdown of the mitochondrial electron transport chain (ETC) subunit cytochrome *c* oxidase-1 (*cco-1*) can induce the UPR^{mt} in the intestine, which promotes longevity and stress resistance (Durieux et al., 2011). In addition, neuronal expression of the Huntington's-disease-causing polyglutamine protein (Q40) not only results in neurotoxicity but also activates the UPR^{mt} in the intestine (Berendzen et al., 2016). Neuronal depletion of the *C. elegans* mitofusin (FZO-1) also induces the intestinal UPR^{mt} activation and alters mitochondrial morphology in peripheral tissues (Chen et al., 2021). Mild mitochondrial stress in

hypothalamic proopiomelanocortin (POMC) neurons in mice enhances thermogenesis and activates the UPR^{mt} in distal adipose tissues, protecting mice from defects in glucose metabolism for obese mice (Kang et al., 2021). Induced ablation of the mitochondrial fission protein Drp1 in the adult forebrain activates the integrated stress response (ISR) and induces the release of FGF21, a cytokine that has been linked to the impaired mitochondrial function in peripheral tissues, into blood circulation (Restelli et al., 2018; Suomalainen et al., 2011).

It has been proposed that a secreted signal (a mitokine) is released from tissues with mitochondrial stress and transmits stress cues to distal tissues (Berendzen et al., 2016; Durieux et al., 2011; Zhang et al., 2018). Recent advances have been made to identify the mitokines that mediate the systemic UPR^{mt} activation. The neurotransmitter serotonin and several neuropeptides were found to be required for the cell-non-autonomous UPR^{mt} activation in response to various neuronal mitochondrial stresses; however, serotonin does not seem to act alone for UPR^{mt} activation (Berendzen et al., 2016; Shao et al., 2016). Our previous study identified that retromer-dependent Wnt/EGL-20 secretion is required for the cell-non-autonomous UPR^{mt} activation (Li et al., 2022; Zhang et al., 2018, 2021). Furthermore, the memory of neuronal mitochondrial stress can also be passed on to their descendants by propagating inheritance of elevated levels of mitochondrial DNA within the germ line, enabling offspring with a greater tolerance to stress and a longer lifespan (Zhang and Tian, 2022; Zhang et al., 2021). Therefore, the neuronal control of the systemic UPR^{mt} activation is critical for coordinating organismal mitochondrial homeostasis and metabolic states. However, the mechanism by which the nervous system senses, integrates, and transmits the signal to distal tissues remains largely unknown.

Here, we performed a genetic screen to look for genes that are specifically required for the cell-non-autonomous UPR^{mt} activation. We identified a G-protein-coupled receptor (GPCR) SRZ-75 that is expressed in a pair of ADL (amphid neurons with dual ciliated sensory endings) chemosensory neurons to coordinate the cell-non-autonomous UPR^{mt} activation via the Gαq signaling. Activation of Gαq in the ADL sensory neurons is sufficient to induce the intestinal UPR^{mt}, resulting in an altered metabolic state, improved proteostasis, and enhanced pathogen resistance. Collectively, our results identified that neuronal GPCR signaling coordinates the systematic mitochondrial stress response, leading to organismal-wide stress regulation.

RESULTS

GPCR SRZ-75 is required for cell-non-autonomous UPR^{mt} activation

Neuronal mitochondrial perturbations induce the UPR^{mt} pathway in the intestine via the mitokine Wnt signaling in *C. elegans* (Zhang et al., 2018). Specific expression of the Wnt ligand EGL-20 in the nervous system is sufficient to activate the UPR^{mt} in peripheral tissues, which can be monitored by the redistribution of a transcription factor DVE-1::GFP reporter or the induction of the mitochondrial chaperone *hsp-6p::gfp* reporter in the intestine (Figures 1A and 1C). To investigate specific neuronal signaling required for cell-non-autonomous UPR^{mt} regulation, we performed an ethyl methanesulfonate (EMS) mutagenesis screen to identify genes that are required for the UPR^{mt} activation in the intestine in response to neuronal Wnt/EGL-20 expression. Of the 3,400 mutagenized genomes screened, one of the mutant alleles *yth17* exhibited strong suppression of the UPR^{mt} within the intestine of animals expressing neuronal Wnt/EGL-20 but did not suppress the UPR^{mt} induced by intestinal Wnt/EGL-20 expression (Figures 1A–1D). Whole-genome deep sequencing indicates that *yth17* carries a mutation in *srz-75* (Ala120Val), an uncharacterized GPCR. Next, we generated a large-deletion mutation (709 bp) in *srz-75(yth75)* via CRISPR-Cas9-mediated gene editing. To our surprise, unlike the point mutation of *srz-75(yth17)*, *srz-75(yth75)* deletion mutants did not exhibit suppression of the UPR^{mt} within the intestine of animals expressing neuronal Wnt/EGL-20 (Figures S1A–S1C). To confirm this result, we generated the same point mutation as *srz-75(yth17)* (Ala120Val) in a wild-type background and crossed it with animals expressing neuronal Wnt/EGL-20 and confirmed that the *yth17* mutation indeed suppressed the intestinal UPR^{mt} activation (Figures S1D and S1E). The mRNA level of *srz-75* was significantly decreased in the *srz-75*(yth17) mutant (Figure S1F). Furthermore, knocking down of *srz-75* by double-stranded RNA (*srz-75p::dsRNA-srz-75*) strongly suppressed the intestinal UPR^{mt} activation in response to neuronal Wnt/EGL-20 expression of the *sid-1* mutants, in which the uptake of extracellular double-stranded RNAs by non-*srz-75*-expressing cells was defective (Winston et al., 2002; Figures S1G–S1J). Together, loss-of-function mutation in *srz-75* suppressed the systemic UPR^{mt} activation in response to neuronal Wnt expression.

The endoplasmic reticulum unfolded protein response (UPR^{ER}) and the cytosolic unfolded protein response (UPR^{cyt}) also function in a cell-non-autonomous manner to coordinate the systemic stress response between different tissues (Morimoto, 2020; O'Brien and van Oosten-Hawle, 2016; Taylor et al., 2014). Neuronal expression of the UPR^{ER} transcription factor *xbp-1s* induces the UPR^{ER} in the intestine (Ron and Walter, 2007; Taylor and Dillin, 2013). Similarly, expression of the UPR^{cyt} transcription factor *hsf-1* in neurons also activates the UPR^{cyt} in the intestine (Douglas et al., 2015; Link et al., 1999). We found that *srz-75(yth17)* was not required for the cell-non-autonomous induction of neither UPR^{ER} nor UPR^{cyt} (Figures S1K–S1N). Thus, *srz-75* appears to be specifically required for cell-non-autonomous UPR^{mt} signaling.

SRZ-75 mediates the systemic UPR^{mt} signaling in ADL chemosensory neurons

To further study how SRZ-75 mediates the systemic UPR^{mt} signaling, we next examined the expression pattern of *srz-75*. We observed that the expression of *srz-75* is limited to a pair of ADL chemosensory neurons in the head region via co-localization analyses of the *srz-75p::mCherry* reporter with multiple neuronal markers (Bargmann, 2006; McCarroll et al., 2005; McGrath et al., 2011; Ortiz et al., 2006; Troemel et al., 1997; Yu et al., 1997; Figures 2A, 2B, S2A, and S2B). Furthermore, both the expression of *srz-75* with its native promoter and ADL-specific promoter *srh-220p* strongly rescued the suppression of the DVE-1::GFP signals in the intestine of *srz-75(yth17)* mutants with neuronal Wnt/EGL-20 expression (Figures 2C and 2D), suggesting that SRZ-75 mediates the systemic UPR^{mt} activation in ADL neurons.

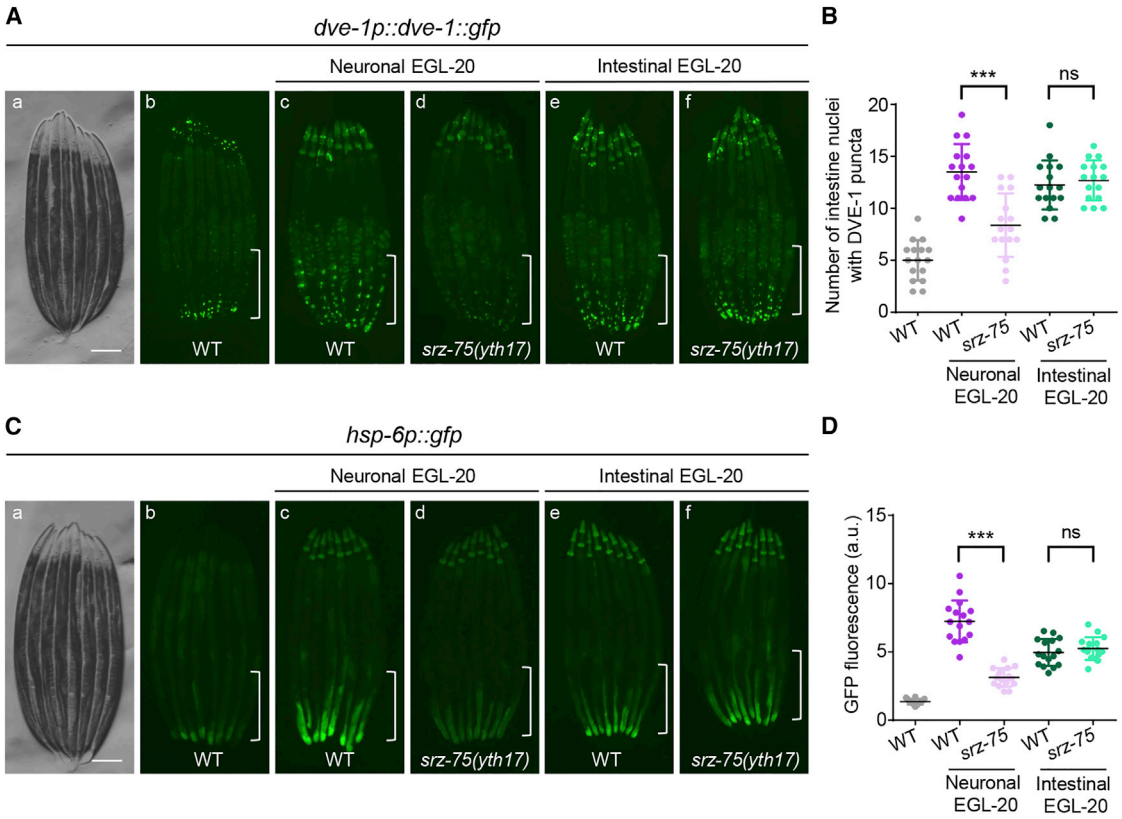

Figure 1. The G-protein-coupled receptor SRZ-75 is required for the systemic UPR^{mt} activation

(A) Representative photomicrographs demonstrating: (Aa) bright-field images of aligned, wild-type (WT) animals; (Ab) the expression pattern of *dve-1p::dve-1::gfp*; (Ac) *dve-1p::dve-1::gfp* expression in *rgef-1p::egl-20* animals; (Ad) *dve-1p::dve-1::gfp* expression in *rgef-1p::egl-20; srz-75(yth17)* animals; (Ae) *dve-1p::dve-1::gfp* expression in *gly-19p::egl-20* animals; and (Af) *dve-1p::dve-1::gfp* expression in *gly-19p::egl-20; srz-75(yth17)* animals. The posterior region of the intestine where DVE-1::GFP is induced or suppressed is highlighted.

(B) Quantification of the number of intestinal nuclei with DVE-1::GFP puncta per worm. The genotypes are as depicted in (A).

(C) Representative photomicrographs demonstrating: (Ca) bright-field images of aligned, WT animals; (Cb) *hsp-6p::gfp* expression pattern; (Cc) *hsp-6p::gfp* expression in *rgef-1p::egl-20* animals; (Cd) *hsp-6p::gfp* expression in *rgef-1p::egl-20; srz-75(yth17)* animals; (Ce) *hsp-6p::gfp* expression in *gly-19p::egl-20* animals; (Cf) *hsp-6p::gfp* expression in *gly-19p::egl-20; srz-75(yth17)* animals. The posterior region of the intestine where *hsp-6p::gfp* is induced or suppressed is highlighted.

(D) Quantification of *hsp-6p::gfp* expression in the entire intestine of animals as depicted in (C).

***$p < 0.001$, ns denotes $p > 0.05$ via unpaired two-tailed Student's t test. Error bars, SEM. $n \geq 15$ worms. Scale bars, 250 μm.

See also Figure S1.

Overexpression of SRZ-75 is sufficient to induce UPR^{mt} in the intestine

We next examined whether overexpression of SRZ-75 was sufficient to induce the UPR^{mt} in the intestine. To this end, we generated transgenic animals overexpressing *srz-75* in ADL neurons with its endogenous promoter *srz-75p*, or the intestinal specific promoter *gly-19p*. Intriguingly, the expression of SRZ-75 in restricted ADL neurons was sufficient to induce UPR^{mt} in the intestine, whereas expression of SRZ-75 in the intestine failed to induce UPR^{mt} (Figures 2E, 2F, and S2C–S2F). In contrast, overexpression of SRZ-75 in ADL neurons did not induce neither the UPR^{ER} nor the UPR^{cyt} (Figures S2G–S2J). qPCR analyses confirmed the activation of endogenous UPR^{mt} target genes in animals overexpressing *srz-75* in ADL neurons (Figure 2G). Moreover, the systemic UPR^{mt} activation in response to ADL-expressing SRZ-75 requires the core components of the UPR^{mt} machinery, such as the transcription factor *atfs-1* and epigenetic regulators *dve-1*, *lin-65*, and the NuRD component *lin-40* (Figures 2H and 2I).

Previous reports have shown that activation of the UPR^{mt} requires a small timing window (L3/L4 stage) during development in *C. elegans* to induce UPR^{mt} (Dillin et al., 2002; Durieux et al., 2011; Rea et al., 2007). We next examined the timing requirement for ADL-expressing SRZ-75 to induce the intestinal UPR^{mt}. To this end, we employed a tissue-specific and heat-shock inducible system in which we could control the timing of *srz-75* expression by heat and limit the expression of the heat-shock transcription factor HSF-1 in the ADL neurons (Bacaj and Shaham, 2007; Yin et al., 2017; Figure 2J). We found that inducing *srz-75* expression during early development (L2–L3, L4; 45 min at 34°C) strongly activated the UPR^{mt} in the intestine. In contrast, inducing *srz-75* expression during adulthood only was unable to induce the UPR^{mt} (Figures 2K and 2L). These results suggest that SRZ-75 functions in ADL

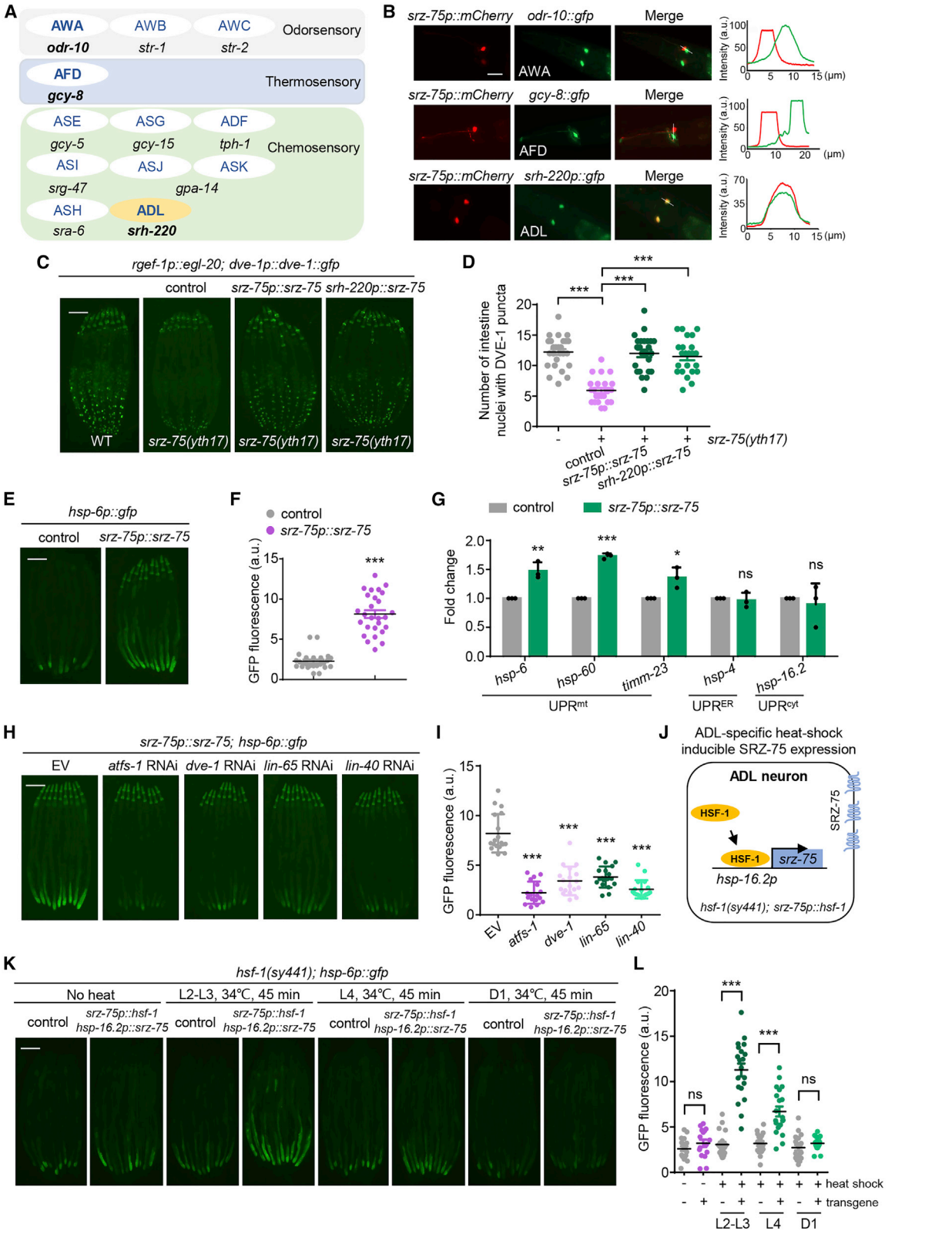

(legend on next page)

neurons during development to coordinate the systemic UPR^{mt} signaling.

SRZ-75 couples with Gαq signaling to transmit the cell-non-autonomous UPR^{mt} signaling

GPCRs transduce extracellular stimuli through the interaction with heterotrimeric G proteins, which are composed of three subunits: α, β, and γ. G-protein functional diversity relies primarily on which α-subunit is used (Bastiani and Mendel, 2006; Yang et al., 2021; Figure 3A). To determine which Gα protein couples with SRZ-75, we introduced loss-of-function mutations in a range of genes required for different Gα signaling pathways in animals expressing neuronal Wnt/EGL-20 and monitored their UPR^{mt} activation. We found that *unc-73(e936)*, an ortholog of mammalian Trio, a guanine nucleotide exchange factor (GEF) that functions downstream of Gαq/EGL-30, but not the Gαs signaling pathway component *acy-1(nu329)* strongly attenuated the induction of the intestinal UPR^{mt} in animals with neuronal Wnt/EGL-20 expression (McMullan et al., 2012; Saifee et al., 2011; Williams et al., 2007; Figures S3A and S3B). We confirmed these results by knocking down *egl-30*(Gαq) or *gsa-1(Gαs)* exclusively in the ADL neurons using a tissue-specific dsRNAi method (the ADL-specific *srz-3* promoter was selected according to the CeNGENApp web application: https://cengen.shinyapps.io/CengenApp/; Taylor et al., 2021) (Figures 3B, 3C, and S3C). We confirmed the results by knocking out Gαq exclusively in the ADL neurons using the tissue-specific CRISPR technique (Figures 3D–3F). The other Gα proteins that were reported to be expressed in ADL neurons (*gpa-1, gpa-3, gpa-11*, and *gpa-15*) are not required for cell-non-autonomous UPR^{mt} activation in response to Wnt/EGL-20 expression (Bargmann, 2006; Bastiani and Mendel, 2006; Figures S3D and S3E). Additionally, the Gαq signaling component *unc-73* was not required for neither the cell-non-autonomous induction of UPR^{ER} nor UPR^{cyt} (Figures S3F and S3G). Together, these results suggest that Gαq signaling in the ADL neurons is required for cell-non-autonomous UPR^{mt} activation in response to neuronal Wnt/EGL-20.

We next examined whether Gαq signaling is required for other forms of cell-non-autonomous UPR^{mt} activation. To our surprise, *acy-1*, but not *unc-73* mutants strongly attenuated the intestinal UPR^{mt} activation in animals with either the neuronal Q40 expression or neuronal *cco-1* knockdown (Figures S3H–S3K), suggesting that different forms of neuronal mitochondrial stresses might elicit the systemic UPR^{mt} via different neuronal GPCR signaling pathways.

To test whether constitutive activation of Gαq and Gαs signaling in the nervous system could trigger the systemic UPR^{mt}, we overexpressed gain-of-function (*gf*) mutations of *Gαq* and *Gαs* in different tissues and examined the UPR^{mt} levels. Notably, pan-neuronal expression of *Gαq(gf)* and *Gαs(gf)* strongly activated UPR^{mt} in the intestine; however, intestinal expression of *Gαq(gf)* and *Gαs(gf)* failed to induce UPR^{mt} (Figures S3L and S3M), suggesting that both neuronal Gαq and Gαs signaling are sufficient to drive UPR^{mt} activation in the intestine. Given that Gαq is required for the systemic UPR^{mt} activation in response to the ADL-expressing SRZ-75 (Figures 3G and 3H), we next activated Gαq signaling specifically in ADL neurons. Remarkably, we found that expression of *Gαq(gf)* in just ADL neurons was sufficient to drive the intestinal UPR^{mt} activation (Figures 3I and 3J). The cell-non-autonomous UPR^{mt} activation caused by enhanced Gαq signaling in the ADL neurons relied on its downstream factor *unc-73* but not *srz-75*, confirming that Gαq acts downstream of SRZ-75 (Figures 3I, 3J, S3N, and S3O). Moreover, qPCR analyses confirmed that the mRNA levels of endogenous UPR^{mt} targeted genes were significantly upregulated in animals with ADL-Gαq activation (Figure 3K). In contrast, the UPR^{ER} reporter *hsp-4p::gfp* and the UPR^{cyt} reporter *hsp-16.2p::gfp* were not induced in these animals (Figures S3P–S3S). Collectively, these results indicate that SRZ-75 couples with the Gαq signaling pathway to drive the systemic UPR^{mt} activation.

Releasing neuropeptides from ADL neurons is essential for cell-non-autonomous UPR^{mt} activation

Activated Gαq directly binds to downstream effectors, initiating cellular signal transduction cascades to mediate diverse cellular processes by promoting the release of neurotransmitters or neuropeptides (Lackner et al., 1999; Sánchez-Fernández et al., 2014). We next examined whether neuroendocrine secretion is required for the cell-non-autonomous UPR^{mt} activation.

Figure 2. SRZ-75 is expressed in ADL chemosensory neurons to mediate the systemic UPR^{mt} activation

(A) Schematic of sensory neurons classification and their specific expression genes.

(B) Fluorescence images of neurons in strains expressing *srz-75p::mCherry* and reporters for indicated sensory neurons. The fluorescence intensity of mCherry and GFP channels across the white line in the merged images is shown on the right. Scale bar, 20 μm.

(C) Representative photomicrographs of *dve-1p::dve-1::gfp* animals expressing *rgef-1p::egl-20* in WT or *srz-75(yth17)* mutant background with overexpression of *srz-75p::srz-75* or *srh-220p::srz-75*. Scale bar, 250 μm.

(D) Quantifications of numbers of intestinal nuclei with DVE-1::GFP puncta in animals as depicted in (C).

(E) Representative photomicrographs of *hsp-6p::gfp* animals in control or *srz-75p::srz-75* background. Scale bar, 250 μm.

(F) Quantification of *hsp-6p::gfp* expression of the entire intestine in animals as depicted in (E).

(G) qRT-PCR of the endogenous transcription levels of *hsp-6*, *hsp-60*, *timm-23*, *hsp-4*, and *hsp-16.2*. Synchronized early L4 larvae of control and *srz-75p::srz-75* animals were collected for qPCR. n = 3.

(H) Representative photomicrographs of *hsp-6p::gfp* animals expressing *srz-75p::srz-75* grown on empty vector (EV), *atfs-1*, *dve-1*, *lin-65*, or *lin-40* RNAi bacteria upon hatching. Scale bar, 250 μm.

(I) Quantification of *hsp-6p::gfp* expression in the entire intestine of animals as depicted in (H).

(J) Schematic of the heat-shock-inducible expression system in ADL neurons.

(K) Representative photomicrographs of *hsp-6p::gfp* animals in *hsf-1(sy441)* mutant background with *srz-75p::hsf-1* and *hsp-16.2p::srz-75* expression. Synchronized L2-L3, L4 and day 1 animals were placed at 34°C for 45 min and then images were taken at day 2. Scale bar, 250 μm.

(L) Quantification of *hsp-6p::gfp* expression in the entire intestine of animals as depicted in (K).

***p < 0.001, **p < 0.01, *p < 0.05, ns denotes p > 0.05 via unpaired two-tailed Student's t test. Error bars, SEM; n ≥ 15 worms.

See also Figure S2.

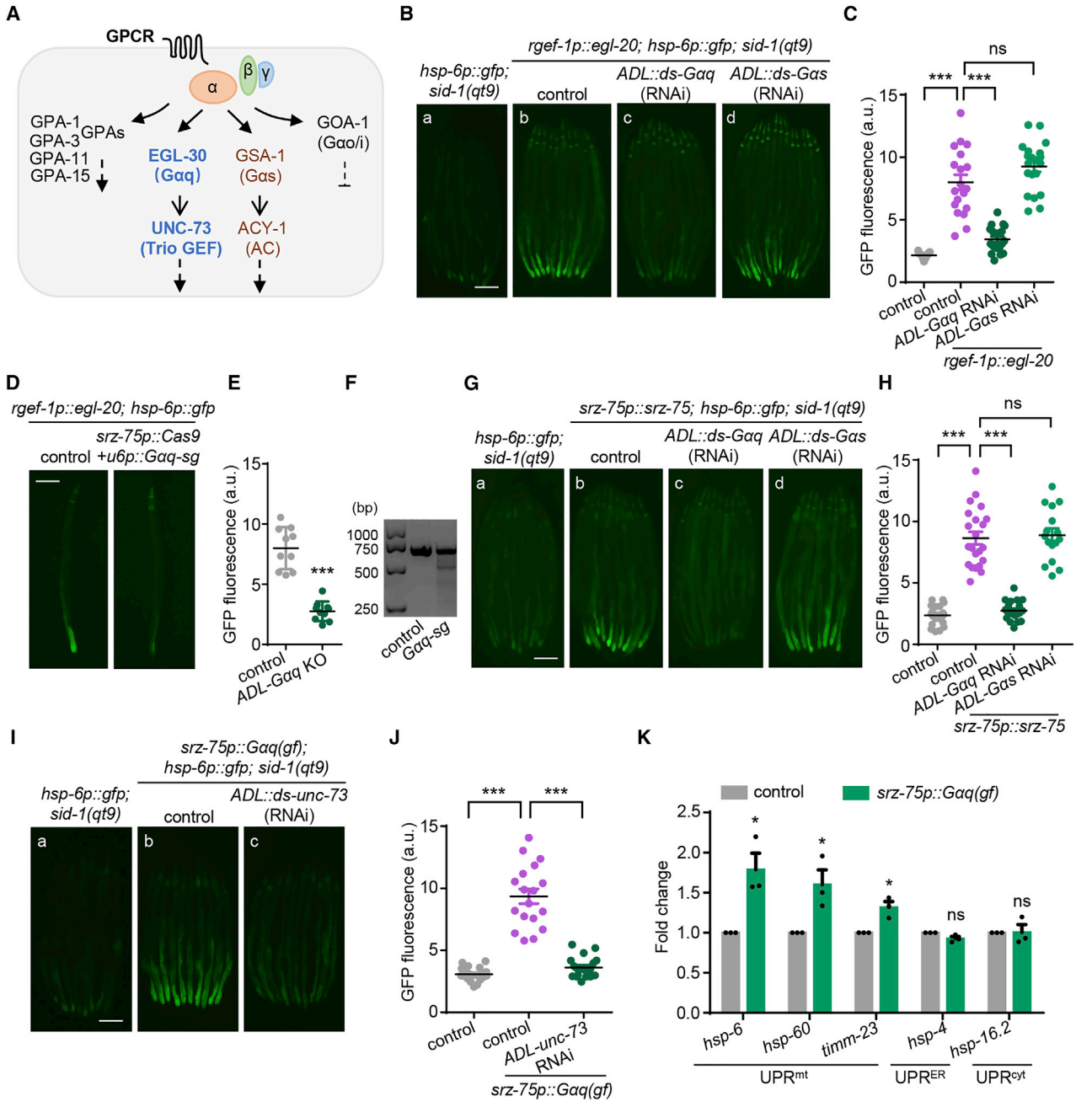

Figure 3. SRZ-75 couples with Gαq signaling in ADL neurons to transmit the UPR^{mt} signal to the intestine

(A) Schematic showing the classification of Gα and their downstream signaling pathways. Gα is composed of GPAs, Gαq, Gαs and Gαo/i.

(B) Representative photomicrographs of *hsp-6p::gfp; sid-1(qt9)* animals in control (Ba), or expressing *srz-75p::srz-75* with control (Bb), *ADL-Gαq* RNAi (Bc), or *ADL-Gαs* RNAi (Bd) background. *ADL-Gαq* and *ADL-Gαs* are knocked down by double-stranded RNA expressed by *srz-3* promoter.

(C) Quantification of *hsp-6p::gfp* expression in the entire intestine of animals as depicted in (B).

(D) Representative photomicrographs of *hsp-6p::gfp* animals expressing *rgef-1p::egl-20* in control or *srz-75p::Cas9+u6p::Gαq-sg* background.

(E) Quantification of *hsp-6p::gfp* expression in the entire intestine of animals as depicted in (D).

(F) Representative DNA gels of T7E1 assay identifies the PCR products amplified from genomic DNA of control worms, or worms with *Gαq* deletion in ADL sensory neurons.

(G) Representative photomicrographs of *hsp-6p::gfp; sid-1(qt9)* animals in control (Ga), or expressing *srz-75p::srz-75* with control (Gb), *ADL-Gαq* RNAi (Gc), or *ADL-Gαs* RNAi (Gd) background.

(H) Quantification of *hsp-6p::gfp* expression in the entire intestine of animals as depicted in (G).

(I) Representative photomicrographs of *hsp-6p::gfp; sid-1(qt9)* animals in control (Ia), or expressing *srz-75p::Gαq(gf, M244I)* with control (Ib), or *ADL-unc-73* RNAi (Ic) background. *ADL-unc-73* is knocked down by double-stranded RNA expressed by *srz-3* promoter.

(legend continued on next page)

We observed that ADL-Gαq activation induced the expression of genes involved in neuropeptide processing, including the proprotein convertase *egl-3*, carboxypeptidase *egl-21*, and the neuroendocrine chaperone 7B2 ortholog *sbt-1* (Husson and Schoofs, 2007; Jacob and Kaplan, 2003; Kass et al., 2001; Figure 4A). In addition, *egl-3* mutant animals that are defective in neuropeptide processing exhibited strong suppression of the intestinal UPR^{mt} activation in response to ADL-Gαq signaling, and the suppression phenotype was partially rescued when restoring EGL-3 function in ADL neurons (Figures 4B and 4C). Furthermore, ADL-specific *egl-3* silencing significantly suppressed the intestinal UPR^{mt} activation in animals with ADL-Gαq activation or neuronal Wnt/EGL-20 expression (Figures S4A–S4D), suggesting that neuropeptides are involved in cell-non-autonomous UPR^{mt} activation. We screened a series of candidate neuropeptide genes that are highly expressed in the ADL neurons (according to the CeNGENApp web application: https://cengen.shinyapps.io/CengenApp/) using the ADL-specific dsRNAi system. The results showed that several genes that encode neuropeptides, such as *nlp-55*, *nlp-67*, *nlp-76*, *daf-28*, and *ins-14*, were required for cell-non-autonomous UPR^{mt} activation in ADL neurons (Figures 4D and 4E; Table S2). Overexpression of *ins-14* and *nlp-76* in just two ADL neurons was also sufficient to activate the UPR^{mt} in the intestine (Figures 4F and 4G).

The neurotransmitter serotonin has been shown to participate in cell-non-autonomous UPR^{mt} activation in animals with a pan-neuronal expression of Q40::YFP or Wnt/EGL-20 (Berendzen et al., 2016; Zhang et al., 2018). However, *tph-1(n4622)* mutants that are deficient in serotonin production did not exhibit suppression of intestinal UPR^{mt} activation in animals with constitutively activated ADL-Gαq (Figures S4E and S4F), suggesting that ADL-Gαq induces the systemic UPR^{mt} in a serotonin-independent manner. Collectively, our results indicate that Gαq activation in ADL neurons drives cell-non-autonomous UPR^{mt} activation via the release of neuropeptides.

Ablation of ADL neurons strongly attenuates the systemic UPR^{mt} activation

Various stress cues act upon specific neuronal subtypes to coordinate different organismal stress responses via distinct secreted neuronal signals (Schiffer et al., 2020). To further investigate whether ADL sensory neurons coordinate the systemic UPR^{mt} activation, we eliminated the ADL neurons during the L1 larval stage in animals and examined the subsequent UPR^{mt} levels in these animals with various neuronal mitochondrial perturbations at day one of adulthood (Alcedo and Kenyon, 2004; Fang-Yen et al., 2012). Notably, we found that laser ablations of ADL neurons strongly suppressed the induction of the UPR^{mt} reporter *hsp-6p::gfp* in the intestine in animals with neuronal Wnt/EGL-20 expression (Figures 5A–5C). Moreover, we could genetically ablate ADL neurons via overexpression of *egl-1*, a cell death activator, in ADL neurons (Conradt and Horvitz, 1998; Yu et al., 2016). We observed that genetic ablation of ADL neurons also significantly suppressed the intestinal UPR^{mt} activation in response to neuronal Wnt/EGL-20 (Figures 5D–5F). Additionally, both laser and genetic ablation of ADL neurons slightly suppressed the intestinal UPR^{mt} activation in animals with neuronal Q40 expression or neuronal *cco-1* knockdown without affecting the baseline level of UPR^{mt} or cell-non-autonomous UPR^{ER} activation (Figures S5A–S5J). Taken together, these results indicated that two ADL chemosensory neurons are essential for coordinating the systemic UPR^{mt} activation.

Enhanced GPCR signaling in ADL neurons alters various physiological characteristics in peripheral tissues

Given that mitochondria are usually targeted by pathogens during infection, metazoans employ mitochondrial surveillance pathways such as the UPR^{mt} to respond to mitochondrial perturbations as an indicator of infection (Jeong et al., 2017; Kwon et al., 2018; Pellegrino et al., 2014; Wang et al., 2018). To explore whether the intestinal activation of UPR^{mt} in response to enhanced GPCR signaling in ADL neurons contributes to pathogen resistance in *C. elegans*, we found that ADL-Gαq animals survived significantly longer than wild-type control animals when exposed to *Pseudomonas aeruginosa* (PA14), a pathogen that kills *C. elegans* within days of exposure (Tan et al., 1999). Furthermore, loss of *atfs-1* suppressed the increased resistance to PA14, suggesting that UPR^{mt} induced by ADL-Gαq is required for host resistance to pathogen infection (Figure 6A). Furthermore, ADL-Gαq-enhanced host resistance to PA14 is dependent on the neuronal control of neuropeptide release from ADL neurons and the subsequent systemic UPR^{mt} activation (Figures 6B and 6C).

UPR^{mt} activation is also coupled to increased mitochondrial proteostasis, which may counteract age-onset proteotoxicity in neurodegenerative diseases (Sorrentino et al., 2017). We found that ADL-Gαq activation significantly decreased the formation of α-synuclein (α-syn) aggregates in muscles cells with age in an established Parkinson's disease (PD) model in *C. elegans* (van Ham et al., 2008; Figures 6D and 6E). The reduction of α-syn aggregates in animals with ADL-Gαq activation was partially dependent on UNC-73 and ADL-EGL-3 but not ATFS-1, suggesting that neuronal control of neuropeptide release but not the systemic UPR^{mt} activation is involved in the improved proteostasis in muscle cells (Figures 6F–6I). Filter trap assays further confirmed that fewer α-syn aggregates formed in animals with ADL-Gαq activation. Moreover, the decline in motility during aging was also significantly delayed in ADL-Gαq animals expressing α-syn (Figures 6J and 6K). Similarly, animals in which SRZ-75 is overexpressed in ADL neurons also exhibited similar improved proteostasis in muscle cells of *C. elegans* (Figures S6A–S6D).

To explore other physiological effects in animals with enhanced GPCR signaling in ADL neurons, we performed mitochondrial functional analyses in these animals. Notably, mitochondria formed a more fragmented and globular structure in

(J) Quantification of *hsp-6p::gfp* expression in the entire intestine of animals as depicted in (I).
(K) qRT-PCR of endogenous transcription levels of *hsp-6*, *hsp-60*, *timm-23*, *hsp-4*, and *hsp-16.2*. Synchronized early L4 larval animals of control and *srz-75p::Gαq(gf)* were collected for qPCR. n = 3.
***p < 0.001, *p < 0.05, ns denotes p > 0.05 via unpaired two-tailed Student's t test. Error bars, SEM; n ≥ 15 worms. Scale bars, 250 μm.
See also Figure S3.

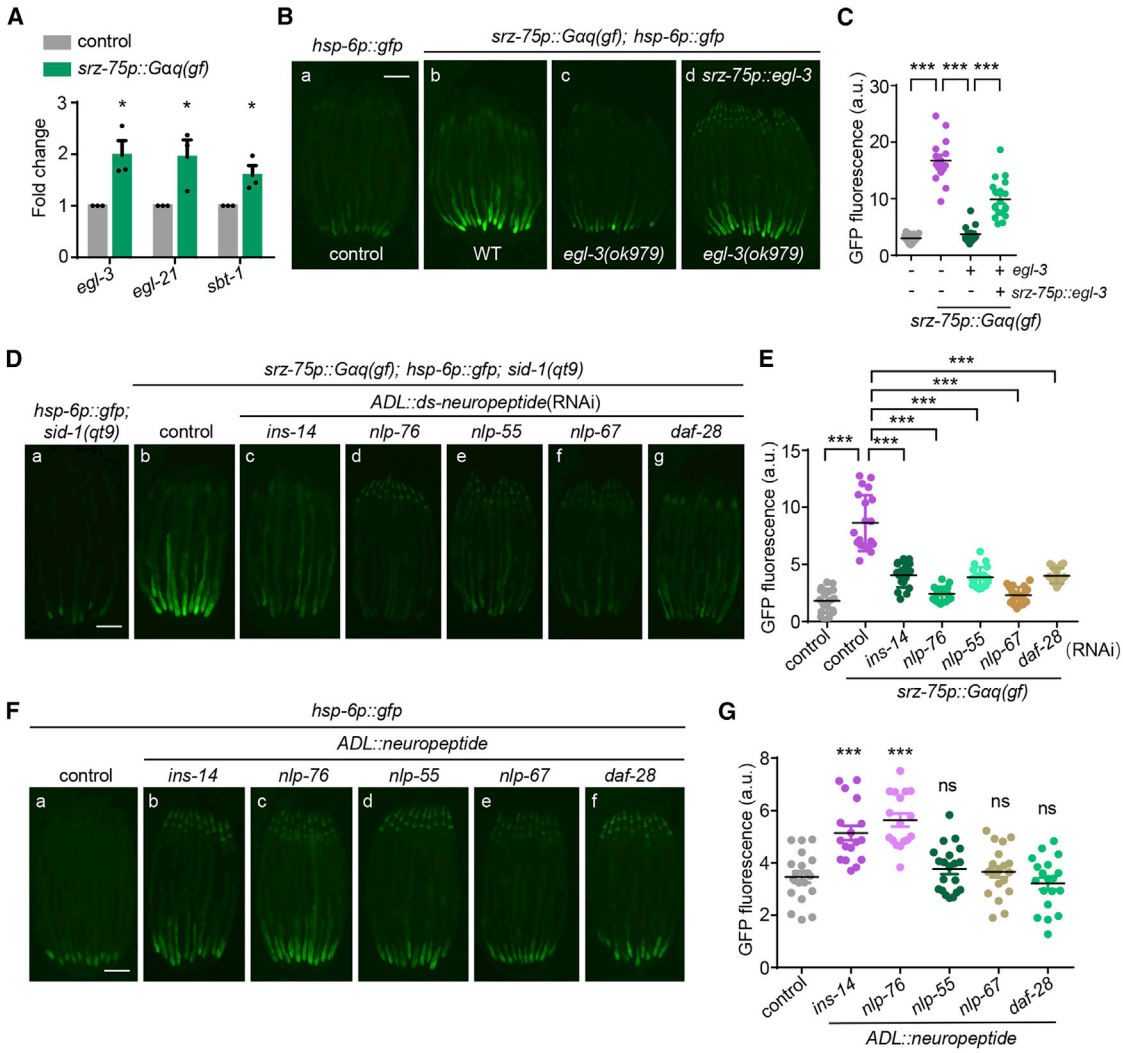

Figure 4. Releasing neuropeptides from ADL neurons is essential for cell-non-autonomous UPR^{mt} activation

(A) qRT-PCR of endogenous transcription levels of *egl-3*, *egl-21*, and *sbt-1*. Synchronized early L4 larval animals of control and *srz-75p::Gαq(gf)* were collected for qPCR. n = 3.

(B) Representative photomicrographs demonstrating: (Ba) *hsp-6p::gfp* expression pattern; (Bb) *hsp-6p::gfp* animals expressing *srz-75p::Gαq(gf)* in WT background; (Bc and Bd) *hsp-6p::gfp* animals expressing *srz-75p::Gαq(gf)* in *egl-3* mutant background with or without *srz-75p::egl-3* overexpression.

(C) Quantification of *hsp-6p::gfp* expression in the entire intestine of animals as depicted in (B).

(D) Representative photomicrographs of *hsp-6p::gfp; sid-1(qt9)* animals in control (Da), or expressing *srz-75p::Gαq(gf)* with control (Db), or (Dc–Dg) *ADL-ins-14*, *nlp-76*, *nlp-55*, *nlp-67* or *daf-28* RNAi background. *ADL-ins-14*, *nlp-76*, *nlp-55*, *nlp-67*, or *daf-28* was knocked down by double-stranded RNA expressed by *srz-3* promoter.

(E) Quantification of *hsp-6p::gfp* expression in the entire intestine of animals as depicted in (D).

(F) Representative photomicrographs of *hsp-6p::gfp* animals in a control (Fa), or (Fb–Ff) expressing *srz-3p::ins-14*, *srz-3p::nlp-76*, *srz-3p::nlp-55*, *srz-3p::nlp-67* or *srz-3p::daf-28*.

(G) Quantification of *hsp-6p::gfp* expression in the entire intestine of animals as depicted in (F).

***p < 0.001, *p < 0.05, ns denotes p > 0.05 via unpaired two-tailed Student's t test. Error bars, SEM; n ≥ 15 worms. Scale bars, 250 μm.

See also Figure S4.

the muscle and hypodermis of animals with constitutive ADL-Gαq activation than the wild-type animals (Figures 6L and 6M). Additionally, these ADL-Gαq animals also exhibited reduced oxygen consumption rates (Figure 6N). Likewise, animals with overexpression of SRZ-75 in ADL neurons also exhibited similar mitochondrial morphology and reduced oxygen consumption rates (Figures S6E–S6G).

Metabolic adaptations inevitably occur during UPR^{mt} activation (Naresh and Haynes, 2019; Valera-Alberni and Canto, 2018). We noted that constitutive ADL-Gαq activation resulted in the reduction of fat storage in the intestine, as assessed by oil red O (ORO) staining (Soukas et al., 2009; Figures 6O and 6P). To test whether the reduction in fat storage was caused by increased lipolysis or decreased lipid synthesis, we

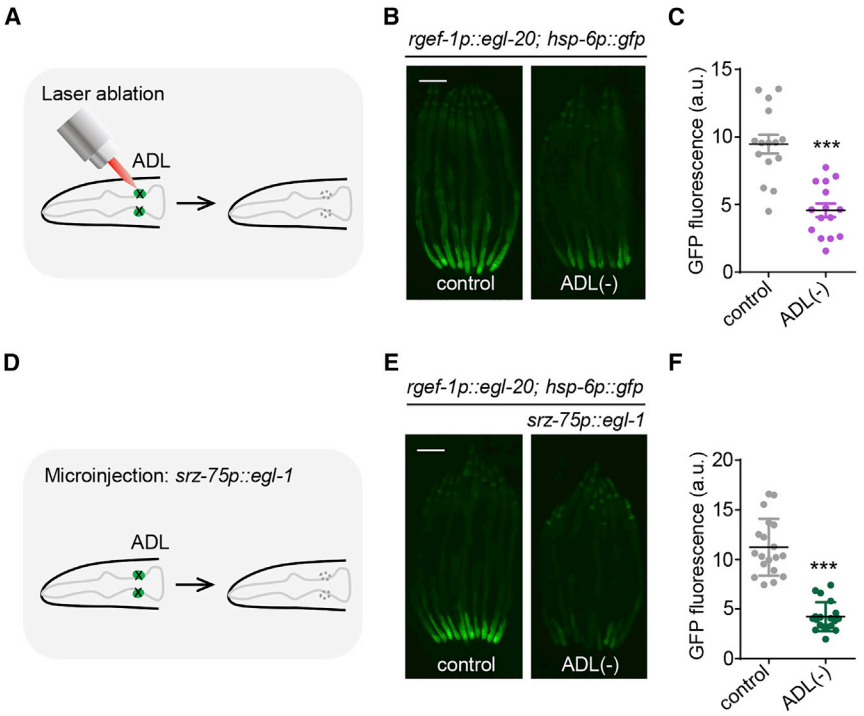

Figure 5. Ablation of ADL neurons attenuates the systemic UPR^{mt} activation

(A) Schematic showing laser ablation of ADL neurons.

(B) Representative photomicrographs of *hsp-6p::gfp* animals expressing *rgef-1p::egl-20* with or without the ablation of ADL neurons. The ablation of ADL neurons could be detected in animals bearing the integrated *srz-75p::mNeonGreen* transgene, as assessed by Zeiss Imager M2 microscope.

(C) Quantification of *hsp-6p::gfp* expression in the entire intestine of animals as depicted in (B).

(D) Schematic showing overexpression of EGL-1 in ADL neurons.

(E) Representative photomicrographs of *hsp-6p::gfp* animals expressing *rgef-1p::egl-20* with or without *srz-75p::egl-1* overexpression. The ablation of ADL neurons could be detected in animals bearing the integrated *srz-75p::mNeonGreen* transgene, as assessed by Zeiss Imager M2 microscope.

(F) Quantification of *hsp-6p::gfp* expression in the entire intestine of animals as depicted in (E).

***$p < 0.001$ via unpaired two-tailed Student's t test. Error bars, SEM; $n \geq 15$ worms. Scale bars, 250 μm.

See also Figure S5.

performed qPCR analyses to examine the expression levels of genes involved in lipid metabolism. ADL-Gαq activation significantly increased the expression of genes involved in lipolysis (*atgl-1*), the mitochondrial fatty acid β-oxidation (*acdh-1* and *cpt-4*), and lipid degradation (*lipl-3*); however, genes involved in lipid synthesis (*fasn-1*, *pod-2*, *dgat-2*, and *fat-5*) were not significantly changed (Figure 6Q). Similarly, animals with overexpressed SRZ-75 also exhibited the reduction of fat storage and showed significant upregulation of lipolysis-related genes (Figures S6H–S6J).

Because animals experiencing mitochondrial stress often exhibit reduced fecundity (Labbadia et al., 2017), we found that animals with ADL-Gαq activation exhibited delayed reproduction and reduced brood size (Figure S6K). Taken together, these results suggest that Gαq activation in a pair of ADL sensory neurons coordinates the systemic mitochondrial stress response and alters various physiological characteristics in peripheral tissues that improve whole-organismal fitness.

DISCUSSION

The nervous system senses stress from external and internal cues and then recruits appropriate effectors to adjust behavioral and physiological responses that promote whole-organism homeostasis (Burkewitz et al., 2015; Gómez-Valadés et al., 2021; Miller et al., 2020). We identified a GPCR SRZ-75 that coordinates the systemic UPR^{mt} activation in a pair of ADL chemosensory neurons of *C. elegans*. Genetically activating GPCR-Gαq signaling in ADL neurons is sufficient to alter various physiological responses in peripheral tissues, promoting proteostasis resistance, and protecting animals against pathogen infection (Figure 7).

To explain the phenotypical discrepancy between a loss-of-function mutation and the null allele, we searched paralogs of SRZ-75 in *C. elegans*. There is a total of 63 paralogs of SRZ-75 in *C. elegans* (www.wormbase.org), and 43 of them are expressed in the ADL neurons (Taylor et al., 2021). There may likely be a functional redundancy when SRZ-75 is absent from the beginning of life.

In the previous studies, the neurotransmitter serotonin was reported to be required for intestinal UPR^{mt} activation due to neuronal Q40::YFP expression (Berendzen et al., 2016). The neuropeptide FLP-2 was found to be necessary and sufficient for intestinal UPR^{mt} activation (Shao et al., 2016). Multiple neurotransmitters and neurohormones were found to be involved in neuronal mitochondrial dynamics that regulate UPR^{mt} in the intestine (Chen et al., 2021). Additionally, GPCR/FSHR-1 is required for the cell autonomous UPR^{mt} activation (Kim and Sieburth, 2020). Our previous studies have shown that neuronal expression of Wnt ligand/EGL-20 induced intestinal UPR^{mt} in a serotonin-dependent manner (Zhang et al., 2018). However, serotonin is not required for cell-non-autonomous UPR^{mt} activation in response to ADL-Gαq signaling, indicating that serotonin might function upstream or in parallel with neuronal GPCR signaling to propagate the UPR^{mt} signal to distal tissues. These studies suggest that neuronal control of the systemic UPR^{mt} activation likely involves multiple distinct neuronal signals in response to various forms of mitochondrial dysfunction.

Mitochondria are desirable targets during pathogen infection, as microbes can produce mitochondrial toxins to exploit mitochondrial function (O'Malley et al., 2003; Pellegrino et al., 2014; Tiku et al., 2020). The premise that the nervous system, experiencing mitochondrial stress, can communicate and transmit stress signals to peripheral tissues is highly reminiscent of

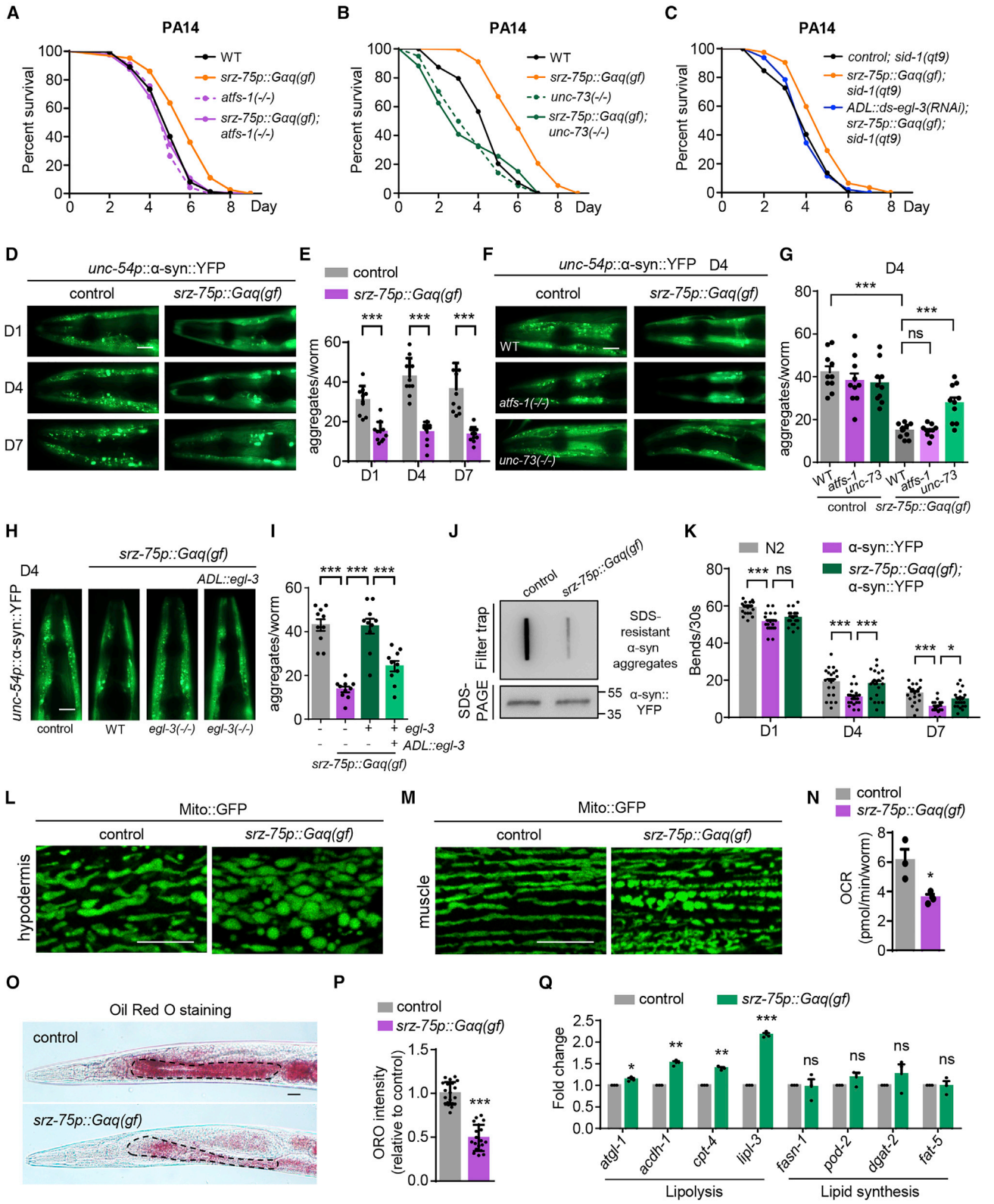

Figure 6. Enhanced Gαq signaling in ADL neurons alters various physiological characteristics in peripheral tissues

(A) Survival analyses of WT, *atfs-1(gk3094)*, *srz-75p::Gαq(gf)*, or *srz-75p::Gαq(gf); atfs-1(gk3094)* animals in the *P. aeruginosa* slow-killing assay.

(B) Survival analyses of WT, *unc-73(e936)*, *srz-75p::Gαq(gf)*, or *srz-75p::Gαq(gf); unc-73(e936)* animals in the *P. aeruginosa* slow-killing assay.

(legend continued on next page)

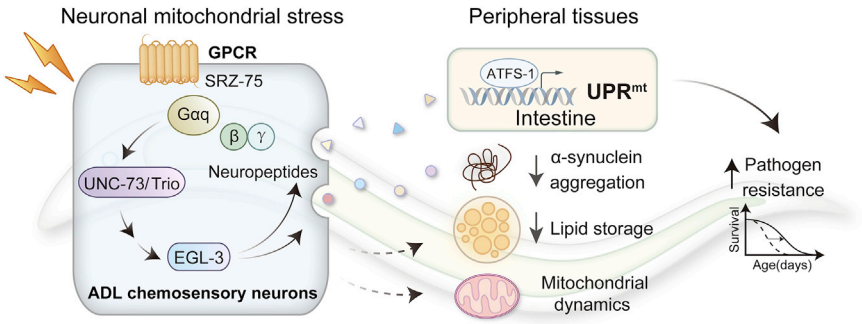

Figure 7. Schematic model of ADL chemosensory neurons coordinating the systemic mitochondrial stress response via GPCR signaling

Two ADL sensory neurons coordinate the inter-tissue UPR^{mt} signaling via SRZ-75-Gαq-neuropeptides pathway. GPCR-Gαq activation in ADL neurons alters different physiological characteristics in distal tissues through multiple distinct signaling pathways.

danger signals that activate immune responses across different tissues. Known to be important for host-pathogen interactions, GPCRs are a class of proteins that can trigger immune responses in various invertebrates (Reboul and Ewbank, 2016; Sun et al., 2011; Zugasti et al., 2014). This suggested that the UPR^{mt} may be regarded as an additional sensor during infection as the pathogen-derived toxins may also lead to mitochondrial dysfunction.

Studies in *C. elegans* have indicated that multiple cellular stressors within neurons can regulate systemic stress responses in distal tissues, promoting the survival of organisms (Durieux et al., 2011; Taylor and Dillin, 2013). However, prolonged exposure to stressors reduced an animal's lifespan (Rodriguez et al., 2013). We found that enhanced GPCR signaling in ADL neurons alters various physiological characteristics in peripheral tissues without affecting the animal's lifespan (Figures S6L and S6M), indicating that neuronal control of lifespan is more complex. It will be interesting to determine whether perpetuating the activation or temporal induction of GPCR signaling in sensory neurons would be beneficial for organismal health and the lifespan in other organisms. Understanding neuronal control of systemic stress response could have potential therapeutic benefits to either enhance the capacity of the proteostasis network when needed during acute stress or prolonged stress, like aging.

Limitations of the study

Our study identifies that a GPCR SRZ-75 couples with Gαq in ADL neurons to drive the systemic UPR^{mt} activation via releasing neuropeptides. However, the ligand for SRZ-75 and the receptors for neuropeptides remain to be determined. Neuronal control of systemic mitochondrial stress response is not limited to a pair of ADL sensory neurons. Our study provides an initial characterization of how a specific GPCR signaling pathway can elicit such broad physiological alterations. Further questions include how neural circuits, specific GPCRs, and additional signaling pathways might fine-tune systemic stress regulation to promote organismal health and aging.

STAR★METHODS

Detailed methods are provided in the online version of this paper and include the following:

- KEY RESOURCES TABLE
- RESOURCE AVAILABILITY
  - Lead contact
  - Materials availability
  - Data and code availability
- EXPERIMENTAL MODEL AND SUBJECT DETAILS

(C) Survival analyses of animals in a control or expressing *srz-75p::Gαq(gf)* with control or *ADL-egl-3* RNAi background in the *P. aeruginosa* slow-killing assay.
(D) Fluorescent images of α-syn aggregates of day 1, day 4, and day 7 adult worms in control or *srz-75p::Gαq(gf)* background. Scale bar, 20 μm.
(E) Quantification of α-syn aggregates larger than 1 μm^2 in the head region of animals as depicted in (D). n = 10 worms.
(F) Fluorescent images of α-syn aggregates of day 4 adult worms in control, *atfs-1* or *unc-73* mutant background with or without *srz-75p::Gαq(gf)* overexpression. Scale bar, 20 μm.
(G) Quantification of α-syn aggregates larger than 1 μm^2 in the head region of animals as depicted in (F). n = 10 worms.
(H) Fluorescent images of α-syn aggregates of day 4 adult worms in control or expressing *srz-75p::Gαq(gf)* with WT or *egl-3* mutant background with or without *srz-3p::egl-3* overexpression. Scale bar, 20 μm.
(I) Quantification of α-syn aggregates larger than 1 μm^2 in the head region of animals as depicted in (H). n = 10 worms.
(J) Filter trap assay of α-synuclein aggregates detected by anti-GFP antibody in control or *srz-75p::Gαq(gf)* background (upper panel). Lower panel: SDS-PAGE analysis with GFP antibody as the loading control.
(K) Motility analysis of N2 and *α-syn::yfp* transgenic worms in control or *srz-75p::Gαq(gf)* background. n = 20 worms.
(L) The mitochondrial morphology in hypodermal cells of animals in control or *srz-75p::Gαq(gf)* background. Scale bar, 10 μm.
(M) The mitochondria morphology in muscular cells of animals in control or *srz-75p::Gαq(gf)* background. Scale bar, 10 μm.
(N) The oxygen consumption rates of animals in control or *srz-75p::Gαq(gf)* background. Synchronized early L4 worms were measured using a Seahorse XFe96 analyzer. n = 3.
(O) Oil red O (ORO) staining of day 1 animals in control or *srz-75p::Gαq(gf)* background. Scale bar, 20 μm.
(P) Quantification of ORO signals from the upper intestine of animals as depicted in (O). n ≥ 15 worms.
(Q) qRT-PCR analysis of endogenous transcription levels of *atgl-1*, *acdh-1*, *cpt-4*, *lipl-3*, *fasn-1*, *pod-2*, *dgat-2,* and *fat-5*. Synchronized day 1 animals in control or *srz-75p::Gαq(gf)* background were collected for qRT-PCR. n = 3.
***p < 0.001, **p < 0.01, *p < 0.05, ns denotes p > 0.05 via unpaired two-tailed Student's t test. Error bars, SEM.
See also Figure S6.

SUPPLEMENTAL INFORMATION

Supplemental information can be found online at https://doi.org/10.1016/j.devcel.2022.10.001.

ACKNOWLEDGMENTS

We thank Tian lab members and Yating Liu for assistance with strain maintenance and reporter crosses. We thank the Bio-imaging Facility of the Institute of Genetics and Developmental Biology Chinese Academy of Science for assisting us with laser ablation experiments using a Zeiss LSM 780 microscope. We are grateful to Yu Wang for her help with acquiring images. Several *C. elegans* strains used in this work were provided by Caenorhabditis Genetics Center (CGC), which is supported by the NIH-Officer of Research Infrastructure Programs (P40 OD010440). Several deletion worm strains were also provided by the Japanese National BioResource Project. Y.T. was supported by the National Key R&D Program of China (2017YFA0506400), Strategic Priority Research Program of Chinese Academy of Sciences (XDB39000000), the CAS Project for Young Scientists in Basic Research (YSBR-076), and the National Natural Science Foundation of China (no. 31930023). X.W. was supported by the Youth Innovation Promotion Association CAS (no. 2021094). Q.Z. was supported by the China National Postdoctoral Program for Innovative Talents (BX2021356) and the China Postdoctoral Science Foundation (2021M703474).

AUTHOR CONTRIBUTIONS

Y.T. and Y.L. conceived the study and designed the experiments. Y.L., J.Z., and N.Z. performed the *C. elegans* crosses, lifespan experiments, the transgene construction, and mitochondrial morphology imaging experiments. Y.L. and J.Z. performed western blotting, filter trap, stress-resistance assay, OCR measurement, and data analysis. Y.L., X.W., and W.Z. performed qPCR experiments. Y.L. performed the CRISPR-Cas9-mediated gene editing and behavior experiments. Y.L., Q.Z., and X.L. performed the EMS mutagenesis screen. Y.T., Y.L., and J.Z. wrote the manuscript.

DECLARATION OF INTERESTS

The authors declare no competing interests.

Received: January 18, 2022
Revised: August 11, 2022
Accepted: October 4, 2022
Published: October 28, 2022

REFERENCES

Alcedo, J., and Kenyon, C. (2004). Regulation of C. elegans longevity by specific gustatory and olfactory neurons. Neuron *41*, 45–55.

Andréasson, C., Ott, M., and Büttner, S. (2019). Mitochondria orchestrate proteostatic and metabolic stress responses. EMBO Rep. *20*, e47865.

Arribere, J.A., Bell, R.T., Fu, B.X., Artiles, K.L., Hartman, P.S., and Fire, A.Z. (2014). Efficient marker-free recovery of custom genetic modifications with CRISPR/Cas9 in *Caenorhabditis elegans*. Genetics *198*, 837–846.

Bacaj, T., and Shaham, S. (2007). Temporal control of cell-specific transgene expression in *Caenorhabditis elegans*. Genetics *176*, 2651–2655.

Bargmann, C.I. (2006). Chemosensation. In C. elegans (October 25, 2006), WormBook., ed. (WormBook: The C. elegans Research Community). https://doi.org/10.1895/wormbook.1.123.1 http://www.wormbook.org.

Bar-Ziv, R., Bolas, T., and Dillin, A. (2020). Systemic effects of mitochondrial stress. EMBO Rep. *21*, e50094.

Bastiani, C., and Mendel, J. (2006). Heterotrimeric G proteins. In C. elegans (October 13, 2006), WormBook., ed. (WormBook: The C. elegans Research Community). https://doi.org/10.1895/wormbook.1.75.1 http://www.wormbook.org.

Berendzen, K.M., Durieux, J., Shao, L.W., Tian, Y., Kim, H.E., Wolff, S., Liu, Y., and Dillin, A. (2016). Neuroendocrine coordination of mitochondrial stress signaling and proteostasis. Cell *166*, 1553–1563.e10.

Burkewitz, K., Morantte, I., Weir, H.J.M., Yeo, R., Zhang, Y., Huynh, F.K., Ilkayeva, O.R., Hirschey, M.D., Grant, A.R., and Mair, W.B. (2015). Neuronal CRTC-1 governs systemic mitochondrial metabolism and lifespan via a catecholamine signal. Cell *160*, 842–855.

Calculli, G., Lee, H.J., Shen, K., Pham, U., Herholz, M., Trifunovic, A., Dillin, A., and Vilchez, D. (2021). Systemic regulation of mitochondria by germline proteostasis prevents protein aggregation in the soma of C. elegans. Sci. Adv. *7*, eabg3012.

Chen, L.T., Lin, C.T., Lin, L.Y., Hsu, J.M., Wu, Y.C., and Pan, C.L. (2021). Neuronal mitochondrial dynamics coordinate systemic mitochondrial morphology and stress response to confer pathogen resistance in C. elegans. Dev. Cell *56*, 1770–1785.e12.

Conradt, B., and Horvitz, H.R. (1998). The C. elegans protein EGL-1 is required for programmed cell death and interacts with the Bcl-2-like protein CED-9. Cell *93*, 519–529.

Dillin, A., Hsu, A.L., Arantes-Oliveira, N., Lehrer-Graiwer, J., Hsin, H., Fraser, A.G., Kamath, R.S., Ahringer, J., and Kenyon, C. (2002). Rates of behavior and aging specified by mitochondrial function during development. Science *298*, 2398–2401.

Douglas, P.M., Baird, N.A., Simic, M.S., Uhlein, S., McCormick, M.A., Wolff, S.C., Kennedy, B.K., and Dillin, A. (2015). Heterotypic signals from neural HSF-1 separate thermotolerance from longevity. Cell Rep. *12*, 1196–1204.

Durieux, J., Wolff, S., and Dillin, A. (2011). The cell-non-autonomous nature of electron transport chain-mediated longevity. Cell *144*, 79–91.

Fang-Yen, C., Gabel, C.V., Samuel, A.D., Bargmann, C.I., and Avery, L. (2012). Laser microsurgery in *Caenorhabditis elegans*. Methods Cell Biol. *107*, 177–206.

Frakes, A.E., and Dillin, A. (2017). The UPR(ER): sensor and coordinator of organismal homeostasis. Mol. Cell *66*, 761–771.

Gómez-Valadés, A.G., Pozo, M., Varela, L., Boudjadja, M.B., Ramírez, S., Chivite, I., Eyre, E., Haddad-Tóvolli, R., Obri, A., Milà-Guasch, M., et al. (2021). Mitochondrial cristae-remodeling protein OPA1 in POMC neurons couples Ca(2+) homeostasis with adipose tissue lipolysis. Cell Metab. *33*, 1820–1835.e9.

Haynes, C.M., Petrova, K., Benedetti, C., Yang, Y., and Ron, D. (2007). ClpP mediates activation of a mitochondrial unfolded protein response in C. elegans. Dev. Cell *13*, 467–480.

Houtkooper, R.H., Mouchiroud, L., Ryu, D., Moullan, N., Katsyuba, E., Knott, G., Williams, R.W., and Auwerx, J. (2013). Mitonuclear protein imbalance as a conserved longevity mechanism. Nature *497*, 451–457.

Husson, S.J., and Schoofs, L. (2007). Altered neuropeptide profile of *Caenorhabditis elegans* lacking the chaperone protein 7B2 as analyzed by mass spectrometry. FEBS Lett. *581*, 4288–4292.

Jacob, T.C., and Kaplan, J.M. (2003). The EGL-21 carboxypeptidase E facilitates acetylcholine release at *Caenorhabditis elegans* neuromuscular junctions. J. Neurosci. *23*, 2122–2130.

Jeong, D.E., Lee, D., Hwang, S.Y., Lee, Y., Lee, J.E., Seo, M., Hwang, W., Seo, K., Hwang, A.B., Artan, M., et al. (2017). Mitochondrial chaperone HSP-60 regulates anti-bacterial immunity via p38 MAP kinase signaling. EMBO J. *36*, 1046–1065.

Kang, G.M., Min, S.H., Lee, C.H., Kim, J.Y., Lim, H.S., Choi, M.J., Jung, S.B., Park, J.W., Kim, S., Park, C.B., et al. (2021). Mitohormesis in hypothalamic POMC neurons mediates regular exercise-induced high-turnover metabolism. Cell Metab. *33*, 334–349.e6.

Kass, J., Jacob, T.C., Kim, P., and Kaplan, J.M. (2001). The EGL-3 proprotein convertase regulates mechanosensory responses of *Caenorhabditis elegans*. J. Neurosci. *21*, 9265–9272.

Kim, S., and Sieburth, D. (2020). FSHR-1/GPCR regulates the mitochondrial unfolded protein response in *Caenorhabditis elegans*. Genetics *214*, 409–418.

Kirienko, N.V., Cezairliyan, B.O., Ausubel, F.M., and Powell, J.R. (2014). Pseudomonas aeruginosa PA14 pathogenesis in *Caenorhabditis elegans*. Methods Mol. Biol. *1149*, 653–669.

Kwon, S., Kim, E.J.E., and Lee, S.V. (2018). Mitochondria-mediated defense mechanisms against pathogens in *Caenorhabditis elegans*. BMB Rep. *51*, 274–279.

Labbadia, J., Brielmann, R.M., Neto, M.F., Lin, Y.F., Haynes, C.M., and Morimoto, R.I. (2017). Mitochondrial stress restores the heat shock response and prevents proteostasis collapse during aging. Cell Rep. *21*, 1481–1494.

Lackner, M.R., Nurrish, S.J., and Kaplan, J.M. (1999). Facilitation of synaptic transmission by EGL-30 Gqalpha and EGL-8 PLCbeta: DAG binding to UNC-13 is required to stimulate acetylcholine release. Neuron *24*, 335–346.

Li, T.Y., Sleiman, M.B., Li, H., Gao, A.W., Mottis, A., Bachmann, A.M., El Alam, G., Li, X., Goeminne, L.J.E., Schoonjans, K., et al. (2021). The transcriptional coactivator CBP/p300 is an evolutionarily conserved node that promotes longevity in response to mitochondrial stress. Nat Aging *1*, 165–178.

Li, X., Li, J., Zhu, D., Zhang, N., Hao, X., Zhang, W., Zhang, Q., Liu, Y., Wu, X., and Tian, Y. (2022). Protein disulfide isomerase PDI-6 regulates Wnt secretion to coordinate inter-tissue UPR(mt) activation and lifespan extension in C. elegans. Cell Rep. *39*, 110931.

Link, C.D., Cypser, J.R., Johnson, C.J., and Johnson, T.E. (1999). Direct observation of stress response in *Caenorhabditis elegans* using a reporter transgene. Cell Stress Chaperones *4*, 235–242.

Mashal, R.D., Koontz, J., and Sklar, J. (1995). Detection of mutations by cleavage of DNA heteroduplexes with bacteriophage resolvases. Nat. Genet. *9*, 177–183.

McCarroll, S.A., Li, H., and Bargmann, C.I. (2005). Identification of transcriptional regulatory elements in chemosensory receptor genes by probabilistic segmentation. Curr. Biol. *15*, 347–352.

McGrath, P.T., Xu, Y., Ailion, M., Garrison, J.L., Butcher, R.A., and Bargmann, C.I. (2011). Parallel evolution of domesticated Caenorhabditis species targets pheromone receptor genes. Nature *477*, 321–325.

McMullan, R., Anderson, A., and Nurrish, S. (2012). Behavioral and immune responses to infection require Galphaq- RhoA signaling in C. elegans. PLoS Pathog. *8*, e1002530.

Miller, H.A., Dean, E.S., Pletcher, S.D., and Leiser, S.F. (2020). Cell non-autonomous regulation of health and longevity. eLife *9*, e62659.

Morimoto, R.I. (2020). Cell-nonautonomous regulation of proteostasis in aging and disease. Cold Spring Harb. Perspect. Biol. *12*, a034074.

Naresh, N.U., and Haynes, C.M. (2019). Signaling and regulation of the mitochondrial unfolded protein response. Cold Spring Harb. Perspect. Biol. *11*, a033944.

Nargund, A.M., Fiorese, C.J., Pellegrino, M.W., Deng, P., and Haynes, C.M. (2015). Mitochondrial and nuclear accumulation of the transcription factor ATFS-1 promotes OXPHOS recovery during the UPR(mt). Mol. Cell *58*, 123–133.

Nargund, A.M., Pellegrino, M.W., Fiorese, C.J., Baker, B.M., and Haynes, C.M. (2012). Mitochondrial import efficiency of ATFS-1 regulates mitochondrial UPR activation. Science *337*, 587–590.

O'Brien, D., and van Oosten-Hawle, P. (2016). Regulation of cell-non-autonomous proteostasis in metazoans. Essays Biochem. *60*, 133–142.

O'Malley, Y.Q., Abdalla, M.Y., McCormick, M.L., Reszka, K.J., Denning, G.M., and Britigan, B.E. (2003). Subcellular localization of Pseudomonas pyocyanin cytotoxicity in human lung epithelial cells. Am. J. Physiol. Lung Cell. Mol. Physiol. *284*, L420–L430.

Ortiz, C.O., Etchberger, J.F., Posy, S.L., Frøkjaer-Jensen, C., Lockery, S., Honig, B., and Hobert, O. (2006). Searching for neuronal left/right asymmetry: genomewide analysis of nematode receptor-type guanylyl cyclases. Genetics *173*, 131–149.

Pellegrino, M.W., Nargund, A.M., Kirienko, N.V., Gillis, R., Fiorese, C.J., and Haynes, C.M. (2014). Mitochondrial UPR-regulated innate immunity provides resistance to pathogen infection. Nature *516*, 414–417.

Pfanner, N., Warscheid, B., and Wiedemann, N. (2019). Mitochondrial proteins: from biogenesis to functional networks. Nat. Rev. Mol. Cell Biol. *20*, 267–284.

Rea, S.L., Ventura, N., and Johnson, T.E. (2007). Relationship between mitochondrial electron transport chain dysfunction, development, and life extension in *Caenorhabditis elegans*. PLoS Biol. *5*, e259.

Reboul, J., and Ewbank, J.J. (2016). GPCRs in invertebrate innate immunity. Biochem. Pharmacol. *114*, 82–87.

Restelli, L.M., Oettinghaus, B., Halliday, M., Agca, C., Licci, M., Sironi, L., Savoia, C., Hench, J., Tolnay, M., Neutzner, A., et al. (2018). Neuronal mitochondrial dysfunction activates the integrated stress response to induce fibroblast growth factor 21. Cell Rep. *24*, 1407–1414.

Rodriguez, M., Snoek, L.B., De Bono, M., and Kammenga, J.E. (2013). Worms under stress: C. elegans stress response and its relevance to complex human disease and aging. Trends Genet. *29*, 367–374.

Ron, D., and Walter, P. (2007). Signal integration in the endoplasmic reticulum unfolded protein response. Nat. Rev. Mol. Cell Biol. *8*, 519–529.

Saifee, O., Metz, L.B., Nonet, M.L., and Crowder, C.M. (2011). A gain-of-function mutation in adenylate cyclase confers isoflurane resistance in *Caenorhabditis elegans*. Anesthesiology *115*, 1162–1171.

Sánchez-Fernández, G., Cabezudo, S., García-Hoz, C., Benincá, C., Aragay, A.M., Mayor, F., Jr., and Ribas, C. (2014). Galphaq signalling: the new and the old. Cell. Signal. *26*, 833–848.

Schiffer, J.A., Servello, F.A., Heath, W.R., Amrit, F.R.G., Stumbur, S.V., Eder, M., Martin, O.M., Johnsen, S.B., Stanley, J.A., Tam, H., et al. (2020). *Caenorhabditis elegans* processes sensory information to choose between freeloading and self-defense strategies. eLife *9*, a033944.

Shao, L.W., Niu, R., and Liu, Y. (2016). Neuropeptide signals cell non-autonomous mitochondrial unfolded protein response. Cell Res. *26*, 1182–1196.

Shao, L.W., Peng, Q., Dong, M., Gao, K., Li, Y., Li, Y., Li, C.Y., and Liu, Y. (2020). Histone deacetylase HDA-1 modulates mitochondrial stress response and longevity. Nat. Commun. *11*, 4639.

Shen, Z., Zhang, X., Chai, Y., Zhu, Z., Yi, P., Feng, G., Li, W., and Ou, G. (2014). Conditional knockouts generated by engineered CRISPR-Cas9 endonuclease reveal the roles of coronin in C. elegans neural development. Dev. Cell *30*, 625–636.

Sorrentino, V., Romani, M., Mouchiroud, L., Beck, J.S., Zhang, H., D'Amico, D., Moullan, N., Potenza, F., Schmid, A.W., Rietsch, S., et al. (2017). Enhancing mitochondrial proteostasis reduces amyloid-beta proteotoxicity. Nature *552*, 187–193.

Soukas, A.A., Kane, E.A., Carr, C.E., Melo, J.A., and Ruvkun, G. (2009). Rictor/TORC2 regulates fat metabolism, feeding, growth, and life span in *Caenorhabditis elegans*. Genes Dev. *23*, 496–511.

Spinelli, J.B., and Haigis, M.C. (2018). The multifaceted contributions of mitochondria to cellular metabolism. Nat. Cell Biol. *20*, 745–754.

Sun, J., Singh, V., Kajino-Sakamoto, R., and Aballay, A. (2011). Neuronal GPCR controls innate immunity by regulating noncanonical unfolded protein response genes. Science *332*, 729–732.

Suomalainen, A., Elo, J.M., Pietiläinen, K.H., Hakonen, A.H., Sevastianova, K., Korpela, M., Isohanni, P., Marjavaara, S.K., Tyni, T., Kiuru-Enari, S., et al. (2011). FGF-21 as a biomarker for muscle-manifesting mitochondrial respiratory chain deficiencies: a diagnostic study. Lancet Neurol. *10*, 806–818.

Tan, M.W., Mahajan-Miklos, S., and Ausubel, F.M. (1999). Killing of *Caenorhabditis elegans* by Pseudomonas aeruginosa used to model mammalian bacterial pathogenesis. Proc. Natl. Acad. Sci. USA *96*, 715–720.

Taylor, R.C., Berendzen, K.M., and Dillin, A. (2014). Systemic stress signalling: understanding the cell non-autonomous control of proteostasis. Nat. Rev. Mol. Cell Biol. *15*, 211–217.

Taylor, R.C., and Dillin, A. (2013). XBP-1 is a cell-nonautonomous regulator of stress resistance and longevity. Cell *153*, 1435–1447.

Taylor, S.R., Santpere, G., Weinreb, A., Barrett, A., Reilly, M.B., Xu, C., Varol, E., Oikonomou, P., Glenwinkel, L., McWhirter, R., et al. (2021). Molecular topography of an entire nervous system. Cell *184*, 4329–4347.e23.

Tian, Y., Garcia, G., Bian, Q., Steffen, K.K., Joe, L., Wolff, S., Meyer, B.J., and Dillin, A. (2016a). Mitochondrial stress induces chromatin reorganization to promote longevity and UPR(mt). Cell *165*, 1197–1208.

Tian, Y., Merkwirth, C., and Dillin, A. (2016b). Mitochondrial UPR: A double-edged sword. Trends Cell Biol. *26*, 563–565.

Tiku, V., Tan, M.W., and Dikic, I. (2020). Mitochondrial functions in infection and immunity. Trends Cell Biol. *30*, 263–275.

Troemel, E.R., Kimmel, B.E., and Bargmann, C.I. (1997). Reprogramming chemotaxis responses: sensory neurons define olfactory preferences in C. elegans. Cell *91*, 161–169.

Valera-Alberni, M., and Canto, C. (2018). Mitochondrial stress management: a dynamic journey. Cell Stress *2*, 253–274.

van Ham, T.J., Thijssen, K.L., Breitling, R., Hofstra, R.M., Plasterk, R.H., and Nollen, E.A. (2008). *C. elegans* model identifies genetic modifiers of alpha-synuclein inclusion formation during aging. PLoS Genet. *4*, e1000027.

Wang, S., Gao, K., and Liu, Y. (2018). UPR(mt) coordinates immunity to maintain mitochondrial homeostasis and animal fitness. Mitochondrion *41*, 9–13.

Williams, S.L., Lutz, S., Charlie, N.K., Vettel, C., Ailion, M., Coco, C., Tesmer, J.J.G., Jorgensen, E.M., Wieland, T., and Miller, K.G. (2007). Trio's Rho-specific GEF domain is the missing Gαq effector in *C. elegans*. Genes Dev. *21*, 2731–2746.

Winston, W.M., Molodowitch, C., and Hunter, C.P. (2002). Systemic RNAi in *C. elegans* requires the putative transmembrane protein SID-1. Science *295*, 2456–2459.

Yang, D., Zhou, Q., Labroska, V., Qin, S., Darbalaei, S., Wu, Y., Yuliantie, E., Xie, L., Tao, H., Cheng, J., et al. (2021). G protein-coupled receptors: structure- and function-based drug discovery. Signal Transduct. Target. Ther. *6*, 7.

Yin, J.A., Gao, G., Liu, X.J., Hao, Z.Q., Li, K., Kang, X.L., Li, H., Shan, Y.H., Hu, W.L., Li, H.P., et al. (2017). Genetic variation in glia-neuron signalling modulates ageing rate. Nature *551*, 198–203.

Yu, S., Avery, L., Baude, E., and Garbers, D.L. (1997). Guanylyl cyclase expression in specific sensory neurons: a new family of chemosensory receptors. Proc. Natl. Acad. Sci. USA *94*, 3384–3387.

Yu, Y., Zhi, L., Guan, X., Wang, D., and Wang, D. (2016). FLP-4 neuropeptide and its receptor in a neuronal circuit regulate preference choice through functions of ASH-2 trithorax complex in *Caenorhabditis elegans*. Sci. Rep. *6*, 21485.

Zhang, Q., and Tian, Y. (2022). Molecular insights into the transgenerational inheritance of stress memory. J. Genet. Genomics *49*, 89–95.

Zhang, Q., Wang, Z., Zhang, W., Wen, Q., Li, X., Zhou, J., Wu, X., Guo, Y., Liu, Y., Wei, C., et al. (2021). The memory of neuronal mitochondrial stress is inherited transgenerationally via elevated mitochondrial DNA levels. Nat. Cell Biol. *23*, 870–880.

Zhang, Q., Wu, X., Chen, P., Liu, L., Xin, N., Tian, Y., and Dillin, A. (2018). The mitochondrial unfolded protein response is mediated cell-non-autonomously by retromer-dependent Wnt signaling. Cell *174*, 870–883.e17.

Zhu, D., Li, X., and Tian, Y. (2022). Mitochondrial-to-nuclear communication in aging: an epigenetic perspective. Trends Biochem. Sci. *47*, 645–659.

Zhu, D., Wu, X., Zhou, J., Li, X., Huang, X., Li, J., Wu, J., Bian, Q., Wang, Y., and Tian, Y. (2020). NuRD mediates mitochondrial stress-induced longevity via chromatin remodeling in response to acetyl-CoA level. Sci. Adv. *6*, eabb2529.

Zugasti, O., Bose, N., Squiban, B., Belougne, J., Kurz, C.L., Schroeder, F.C., Pujol, N., and Ewbank, J.J. (2014). Activation of a G protein-coupled receptor by its endogenous ligand triggers the innate immune response of *Caenorhabditis elegans*. Nat. Immunol. *15*, 833–838.

STAR★METHODS

KEY RESOURCES TABLE

REAGENT or RESOURCE	SOURCE	IDENTIFIER
Antibodies		
Mouse monoclonal anti-GFP mAb(AE012)	ABclonal	Cat#AE012; RRID: AB_2770402
Bacterial and virus strains		
OP50	CGC	N/A
HT115	CGC	N/A
DH5a	Weidi	Cat#DL1001M
Chemicals, peptides, and recombinant proteins		
Ethyl methanesulfonate	Sigma	Cat#M0880
AGAROSE	Life Technology	Cat#202007
Sodium chloride	Sigma	Cat#V900058
Bacto Agar	BD	Cat#214010
Bacto Peptone	BD	Cat#211677
Cholesterol	Sigma	Cat#C8667
Calcium chloride dihydrate	Sigma	Cat#C7902
Magnesium sulfate heptahydrate	Sigma	Cat#M1880
Potassium phosphate monobasic	Sigma	Cat#V900041
Potassium phosphate dibasic	Sigma	Cat#V900050
Sodium phosphate dibasic	Sigma	Cat#V900061
Isopropyl beta-D-thiogalactoside	Sigma	Cat#V900917
Carbenicillin Na2	INALCO	Cat#1758-9317
Potassium hydroxide	Sigma	Cat#221473
GeneGreen	Tiangen	Cat#RT210
TRYPTONE	OXOID	Cat#CM0129
YEAST EXTRACT	OXOID	Cat#LP0021
Sodium azide	Sigma	Cat#S2002
Halocarbon oil 700	Sigma	Cat#H8898
TRIzol	Invitrogen	Cat#15596026
Sodium acetate buffer solution	Sigma	Cat#S7899
FudR	Aladdin	Cat#F110732
Critical commercial assays		
QIAprep Spin Miniprep Kit	Qiagen	Cat#27104
MinElute PCR Purification Kit	Qiagen	Cat#28004
Tanon High-sig ECL Western Blotting Substrate	Tanon	Cat#180-501
KOD-Plus-Neo	Toyobo Life Science Department	Cat#KOD-401
2 x Rapid Taq Master Mix	Vazyme	Cat#P222-03
One Step Cloning Kit	Vazyme	Cat#C112
M-MLV Reverse Transcriptase	Invitrogen	Cat#28025013
RQ1 RNase-Free Dnase	Promega	Cat#M6101
RNasin Ribonuclease Inhibitor	Promega	Cat#N2111
SYBR Green Realtime PCR Master Mix	Toyobo	Cat#QPK-201
Experimental models: Organisms/strains		
See Table S1 for organisms/strains	This study	N/A
Oligonucleotides		
See Table S3 for primer sequences	This study	N/A

(*Continued on next page*)

Continued

REAGENT or RESOURCE	SOURCE	IDENTIFIER
Recombinant DNA		
srz-75p::mCherry	This study	N/A
srz-75p::bfp	This study	N/A
srh-220p::gfp	This study	N/A
srg-47p::gfp	This study	N/A
gcy-15p::gfp	This study	N/A
gpa-14p::gfp	This study	N/A
srz-3p::gfp	This study	N/A
srz-75p::mNeonGreen	This study	N/A
srz-75p::srz-75	This study	N/A
srh-220p::srz-75	This study	N/A
gly-19p::srz-75	This study	N/A
srz-75p::hsf-1	This study	N/A
hsp-16.2p::srz-75	This study	N/A
rgef-1p::Gαq(M244I, gf)	This study	N/A
rgef-1p::Gαs(gf, G48R)	This study	N/A
gly-19p::Gαq(M244I, gf)	This study	N/A
gly-19p::Gαs(gf, G48R)	This study	N/A
srz-75p::Gαq(M244I, gf)	This study	N/A
gly-19p::Gαq(M244I, gf)	This study	N/A
eft-3p::Cas9+u6p::srz-75-sg pDD162	This study	N/A
srz-75p::Cas9+u6p::Gαq-sg pDD162	This study	N/A
srz-75p::egl-3	This study	N/A
srz-3p::egl-3	This study	N/A
srz-75p::srz-75_sense	This study	N/A
srz-75p::srz-75_antisense	This study	N/A
srz-3p::egl-30_sense	This study	N/A
srz-3p::egl-30_antisense	This study	N/A
srz-3p::egl-3_sense	This study	N/A
srz-3p::egl-3_antisense	This study	N/A
srz-75p::egl-1	This study	N/A
srz-3p::egl-1	This study	N/A
srz-3p::ins-14	This study	N/A
srz-3p::nlp-76	This study	N/A
srz-3p::nlp-55	This study	N/A
srz-3p::nlp-67	This study	N/A
srz-3p::daf-28	This study	N/A
Software and algorithms		
GraphPad Prism 6	GraphPad Software	https://www.graphpad.com/scientificsoftware/prism/
ImageJ 1.48v	Wayne Rasband (NIH)	https://imagej.nih.gov/ij/
Zen	Zeiss	https://www.zeiss.com/microscopy/us/products/microscope-software/zen.html

RESOURCE AVAILABILITY

Lead contact

Further information and requests for resources and reagents should be directed to and will be fulfilled by the lead contact, Ye Tian (ytian@genetics.ac.cn).

Materials availability

All unique/stable reagents generated in this study are available from the lead contact with a completed material transfer agreement.

Data and code availability

All data reported in this paper will be shared by the lead contact upon request.

This paper does not report original code.

Any additional information required to reanalyze the data reported in this paper is available from the lead contact upon request.

EXPERIMENTAL MODEL AND SUBJECT DETAILS

Caenorhabditis elegans maintenance and transgenic lines

Nematodes were maintained and experimentally examined at 20°C on standard nematode growth medium agar plates seeded with *Escherichia coli* OP50.

The strains used in this study were obtained from the Caenorhabditis Genome Center (Minneapolis, MN): Bristol (N2) strain as wild-type (WT) strain.

For generation of *srz-75p::mCherry* strain, the *srz-75* 2.2 kb promoter was PCR amplified from genomic DNA and cloned into the vector containing the mCherry and *unc-54* 3′-UTR sequence. For generation of *srz-75p::bfp* strain, the *srz-75* promoter was cloned into the vector containing the bfp and *tbb-2* 3′-UTR sequence. For generation of *srh-220p::gfp*, *srg-47p::gfp*, *gcy-15p::gfp, gpa-14p::gfp* or *srz-3p::gfp*, the *srh-220*, *srg-47*, *gcy-15*, *gpa-14* or *srz-3* promoter was PCR amplified from genomic DNA and inserted into the vector containing the GFP and *unc-54* 3′-UTR sequence. For the *srz-75p::mNeonGreen*, the *srz-75* promoter was inserted into the vector pXH27C containing the mNeonGreen and *unc-54* 3′-UTR sequence. The vector pXH27C was a gift from Prof. Zhuo Du, Institute of Genetics and Developmental Biology, Chinese Academy of Sciences, China. For the plasmid *srz-75p::srz-75*, the *srz-75* 2.2 kb promoter and *srz-75* gDNA with stop codon were PCR amplified from genomic DNA and cloned into vector containing *unc-54* 3′-UTR sequence. For the *hsp-16.2p::srz-75*, *srh-220p::srz-75*, or *gly-19p::srz-75*, the *hsp-16.2*, *srh-220*, or *gly-19* promoter was cloned in place of the *srz-75* promoter in the *srz-75p::srz-75* plasmid. For the plasmid *srz-75p::Gαq(gf, M244I)* or *srz-75p::Gαs(gf, G48R), egl-30* or *gsa-1* cDNA with the amino acid mutation was cloned in place of the *srz-75* gDNA in the *srz-75p::srz-75* plasmid. For the *rgef-1p::Gαq(gf, M244I)*, *gly-19p::Gαq(gf, M244I)*, *rgef-1p::Gαs(gf, G48R)* or *gly-19p::Gαs(gf, G48R)*, the *rgef-1* or *gly-19* promoter was cloned in place of the *srz-75* promoter in the *srz-75p::Gαq(gf, M244I)* or *srz-75p::Gαs(gf, G48R)* plasmid. For the plasmid *srz-75p::hsf-1, srz-75p::egl-3* or *srz-75p::egl-1*, the cDNA of *hsf-1, egl-3* or the gDNA of *egl-1* was cloned in place of the *srz-75* gDNA in the *srz-75p::srz-75* plasmid. For the plasmid *srz-3p::egl-3* or *srz-3p::egl-1*, the *srz-3* promoter was cloned in place of the *srz-75* promoter in the *srz-75p::egl-3* or *srz-75p::egl-1* plasmid.

To generate ADL-neurons-specific *srz-75* knockdown strain, we cloned 0.6 kb fragment of *srz-75* genomic sequence in either sense or anti-sense orientation as separate constructs containing *unc-54* 3′-UTR sequence under the *srz-75* 2.2 kb promoter. To generate ADL-neurons-specific knockdown transgenic strains, we cloned 0.5 kb, 0.7 kb, 0.8 kb and 0.9 kb fragments of *egl-30*, *gsa-1*, *unc-73* and *egl-3* cDNA sequences, respectively, in either sense or anti-sense orientation as separate constructs containing *unc-54* 3′-UTR sequence under the *srz-3* 2 kb promoter. To generate ADL-neurons-specific neuropeptides knockdown transgenic strains, we cloned about 0.4 kb fragments of these neuropeptide cDNA sequences in either sense or anti-sense orientation as separate constructs containing *unc-54* 3′-UTR sequence under the *srz-3* 2 kb promoter.

Transgenic strains were generated by microinjecting target constructs (50 ng/μl) mixed with a pRF4(*rol-6*) (50 ng/μl), a *myo-2p::tdTomato* (25 ng/μl), a *myo-3p::DsRed* (25 ng/μl) or a *str-3p::mCherry* (50 ng/μl) co-injection marker. Integrated lines were generated using UV irradiation and backcrossed six times.

METHOD DETAILS

EMS mutagenesis

The protocol for EMS mutagenesis used was described previously (Houtkooper et al., 2013). Synchronized L4-stage worms were treated with 47 mM EMS (Ethyl Methanesulfonate, Sigma #M-0880) for 4 hours. Worms were washed with M9 and transferred to plates. Healthy late L4 animals were picked off to use as P0. F1 progeny were then allowed to self-fertilize, and F2 animals were screened for the phenotype of interest.

RNAi feeding

Age synchronized worms were bleached and grown from hatch on *Escherichia coli* HT115 strains containing an empty vector control or double-stranded RNA. RNAi strains were from the Vidal library if present, or the Ahringer library if absent from the Vidal library.

CRISPR/Cas9 mediated gene editing

To generate *srz-75(yth17)* mutants, two single-guide RNA (sgRNA) targeting sequence (5'-GAAGCGTTGAGCCGCTAGC-3', 5'-TAG CAGGAATATTAGAAAA-3') of *srz-75* were cloned into the pDD162 vector with the expression of Cas9 enzyme. A repair template containing the mutation of interest and additional silent mutations were designed to remove the cleavage site. *dpy-10* was used as a positive control marker (Arribere et al., 2014). The sgRNA vectors (50 ng/μl) and repair template (2 μM) of *srz-75* mutation were

co-injected with the sgRNA vector (50 ng/μl) and repair template (2 μM) for *dpy-10*. Roller F1 worms were singled into new plates and F2 progeny were examined by PCR amplification and restriction digestion. The mutations were confirmed by sequencing.

To generate *srz-75(yth75)* mutants, two single-guide RNA (sgRNA) targeting sequence (5'-TAAATCCGCTAACTGTCGGT-3', 5'-CAGGTTACTGCCAGGACACG-3') of *srz-75* were cloned into the pDD162 vector with the expression of Cas9 enzyme. The sgRNA vectors (50 ng/μl) of *srz-75* mutation were co-injected with the co-injection marker *myo-2p::tdTomato* (10 ng/μl). F1 worms with expression of *myo-2p::tdTomato* were singled into new plates and F2 progeny were examined by PCR amplification and restriction digestion. The mutations were confirmed by sequencing.

To generate knockout of *Gαq* specifically in ADL neurons, the *eft-3* promoter in the original vector was replaced with *srz-75* pro moter to express Cas9 endonuclease specifically in ADL neurons. Two single-guide RNA (sgRNA) targeting sequence (5'-CATTTT-GAGAATAAACTCG-3', 5'-CCGATGAGTTGGTGAACCA-3') of *egl-30* were cloned into the vector. Conditional knockout strains were generated by microinjecting 50 ng/μl Cas9-sgRNA plasmids with 30 ng/μl co-injection marker *myo-3p::DsRed*.

T7 endonuclease I (T7E1) assay was performed to detect indels produced by *Gαq*-sg (Mashal et al., 1995; Shen et al., 2014). DNA fragments containing target sites were PCR amplified and digested with T7E1 (NEB, #M0302) and analyzed via agarose gel electrophoresis. Non-perfectly matched DNA would be cleaved by T7E1.

Analysis of the fluorescence intensity in whole worm

For fluorescence image, worms were anesthetized with 50 mM sodium azide, and photographs were taken using a Leica M165 FC dissecting microscope. To quantify fluorescent intensity, the entire intestine regions were outlined and quantified using ImageJ software. For quantifying the nuclear localization of DVE-1::GFP, the worms were mounted on 2% agarose pads with 50 mM sodium azide and imaged using Zeiss Imager M2 microscope.

RNA isolation and quantitative PCR analyses

Total RNA was isolated using TRIzol (Invitrogen). Worms were synchronized and washed off the plates using M9 buffer, and 500 μl TRIzol were added to the samples and homogenized by repeated freezing and thawing using liquid nitrogen. RNA was isolated according to manufacturer''s instructions. DNA was wiped off using RQ1 RNase-Free DNase (Promega). cDNA was synthesized using the M-MLV Reverse Transcriptase (Invitrogen). Gene expression levels were determined by real-time PCR using SYBR Green Real-time PCR Master Mix (Toyobo) and Bio-rad CFX96 Real-Time PCR Detection Systems. Relative gene expression was normalized to *act-3* (*T04C12.4*) mRNA levels. Fold changes in gene expression were calculated using the comparative $\Delta\Delta C_t$ method, and then normalized to the control for every single biological repeat. The primer sequences used in the quantitative PCR are shown in Table S3. In each experiment, three biological samples were analyzed.

Laser ablation

Worms at larval 1 (L1) stage were transferred to an agar pad and anesthetized using 50 mM sodium azide. The GFP or mCherry-expressing ADL neurons were killed using a laser microbeam focused through a 100x objective on a Zeiss LSM 780 microscope. The sensory neuron-ablated worms were recovered on OP50 plates and allowed to grow into D2 stage. The ablated worms with a similar growth rate to the unoperated worms were used for subsequent experiments. Ablation was confirmed via the loss of GFP or mCherry signal.

Measurement of oxygen consumption rate

Oxygen consumption rate (OCR) was measured using a Seahorse XFe96 analyzer (Seahorse Bioscience) at 20 °C as described previously (Houtkooper et al., 2013). Synchronized early L4 worms of each strain were collected and washed three times with M9. 20 worms were transferred into each well of a 96-well microplate containing 200 μl M9, 6 wells per strain. Basal respiration was measured for a total of 168 min, in 21-min intervals that included a 3 min mix, a 8 min time delay and a 10 min measurement. Experiments were repeated at least three times for each strain. Student's t-tests were used to determine the level of statistical significance.

Oil-Red-O staining and quantification

Synchronized day 1 worms were collected and washed three times with M9. Worms were suspended in 1 ml M9, and then 100 μl 4% paraformaldehyde (PFA) was added and mixed. Worms were immediately frozen briefly in liquid nitrogen, and subjected to three incomplete freeze/thaw cycles, followed by washing with M9 to remove PFA and resuspension in 60% isopropanol to dehydrate. Worms were incubated with rocking in 60% ORO solution for several hours at room temperature. The 60% ORO solution was prepared as follows: from 0.5 g/100 mL isopropanol stock solution, freshly dilute with water, rock for several hours and filter with a 0.22-μm filter. Stained worms were washed with M9, and then mounted and imaged using a Zeiss Imager M2 microscope. To quantify ORO signals, images were converted to RGB color and the mean intensity in the green color channel of the post pharyngeal intestine was measured using Image J software.

Quantification of aggregation

NL5901 (*pkIs2386[unc-54p::alphasynuclein::yfp + unc-119(+)]*) worms were anaesthetized using 50 mM sodium azide and high magnification (40x objective) images of the head region were obtained by using a Zeiss Imager M2. Fluorescent spots bigger than 1 μm^2, present in the region between the tip of head and the end of the pharyngeal bulb, were quantified and analyzed using ImageJ software.

Filter trap assay

At day 4 of adulthood, worms were collected with M9 buffer. After washing, the animals were resuspended in lysis buffer [50 mM tris-HCl, (pH 7.4), 1 mM EDTA, 150 mM NaCl, and 1% Triton X-100] supplemented with EDTA-free protease inhibitor cocktail (Roche) (Calculli et al., 2021). The suspension was then dripped into liquid N_2, and the resulting balls were grinded using mortar and pestle. Worm debris was removed with 1000*g* spin for 5 min at 4 °C. Based on the results of Western blot analysis, adjust the contents of loading protein extract for filter trap. At least one hundred micrograms of protein extract was supplemented with SDS at a final concentration of 0.5% and loaded onto a nitrocellulose membrane (0.45 μm) assembled in a slot blot apparatus (Bio-Rad). Then, the membrane was washed with 0.2% SDS and SDS-resistant protein aggregates were assessed by immunoblotting using antibodies against GFP (1:1000; ABclonal, AE012).

Western blot

About five micrograms of protein extracts was separated by SDS-PAGE and subjected to immunoblotting. Western blot was performed with anti-GFP antibody (1:1000; ABclonal, AE012).

Motility assay

At day1, day 4 and day 7 of adulthood, worms were transferred to a drop of M9 buffer. After 30 s of adaptation, the number of body bends was counted for 30 s. A body bend was defined as change in the direction of bending in the middle of the body (Calculli et al., 2021).

P. aeruginosa slow-killing assay

Slow-killing experiments were performed as previously described (Kirienko et al., 2014). *P. aeruginosa* was cultured overnight in LB containing 50 μg/ml kanamycin at 37°C. To prepare *P. aeruginosa* plates, 10 μl *P. aeruginosa* was seeded onto 6 cm slow-killing agar plates and spread slightly to a small circle. Plates were incubated at 37°C for 24 h and then incubated at room temperature for another 24 h. To score survival rate of worms, 100 μl 10 mg/ml 5-fluoro-20-deoxyuridine (FUdR) was added in the *P. aeruginosa* plates. Worms were synchronized by egg bleach and were grown on OP50 from hatch. Then, synchronized day 1 worms were transited to slow-killing agar plates and cultured at 25°C. Worms were scored counted every 24 h. All survival data are available in Table S4.

Lifespan analysis

Lifespan experiments were performed on NGM plates at 20°C as previously described (Dillin et al., 2002). To prevent progeny production, 100 μl 10 mg/ml 5-fluoro-20-deoxyuridine (FUdR) was added to seeded plates. Worms were synchronized by egg bleach and were grown on OP50 from hatching, and transited to FUdR plates from L4 to early adulthood. Worms were treated a second time at day 5 of adulthood. Worms were scored every second day. Prism6 software was used for statistical analysis. Log-rank (Mantel-Cox) method was used to determine the significance difference. All survival data are available in Table S4.

Brood size assay

10 synchronized L4 worms were placed onto NGM plates with seeded OP50 at 20°C and transferred to fresh dishes daily until they stopped laying eggs. The total number of progenies was counted for each strain. Five replicates per treatment with two biological repeats.

QUANTIFICATION AND STATISTICAL ANALYSIS

Experiments yielding quantitative data for statistical analyses were performed independently at least three times with similar results. Statistical parameters, including the exact value of n and descriptive statistics (mean ± SEM) and statistical significance are reported in the Figures and the Figure Legends. Data are judged to be statistically significant when $P < 0.05$ by unpaired two-tailed Student's *t* test. In figures, asterisks denote statistical significance as calculated by Student's *t* test (*, $P < 0.05$, **, $P < 0.01$, ***, $P < 0.001$) as compared to appropriate controls. Lifespans and slow-killing assays were analyzed using Mantel-Cox log-rank test.